TAMPEREEN TEKNILLINEN YLIOPISTO
TAMPERE UNIVERSITY OF TECHNOLOGY

SHUAI CHUFAN

FEASIBILITY OF ESTIMATION PROGRAMS FOR HOLE EXPANSION TEST ON SHEET STEEL

Master of Science thesis

Examiners: Associate Professor Pasi Peura and Dr. Mikko Hokka
Examiners and topic approved by the
Faculty Council of the Faculty of Engineering sciences
on 9th of September 2015

ABSTRACT

SHUAI CHUFAN: Feasibility of estimation programs for hole expansion test on sheet steels
Tampere University of technology
Master of Science Thesis, 78 pages, 2 Appendix page
December 2015
Master's Degree Programme in Materials Science
Major: Material Research
Examiners: Associate Professor Pasi Peura and Dr. Mikko Hokka
Keywords: Sheet steel, hole expansion test, estimation, feasibility, artificial neural network, microstructure, fracture

Sheet steels are thin steels with excellent formability and good strength, which have various applications in industrial production. Hole expansion tests, which measure the hole expansion ratio (HER), can represent the formability of sheet steel, especially for highly advanced strength steel. Meanwhile, to increase the accuracy of the test, estimation program is an efficient method which used to predict or examine the test result. However, the feasibility of estimation programs always has fluctuation and due to some inherent defects of programing and training methods, the simulated results from estimation programs might have some extent of differences compared with the test results. Thus, thorough analysis of these differences and accuracy improvement of estimation programs are essential. In this master thesis, five different sheet steels and seven HER estimation programs are selected to analyze the feasibility of the estimation programs.

The thesis includes theoretical, experimental and discussion parts. Theoretical parts will introduce theoretical backgrounds which relate to the thesis topic. Experimental parts comprise tensile tests, hole expansion tests, HER program estimations and microscopy. Except hole expansion tests and part of tensile tests, which were conducted at SSAB Europe (Hämeenlinna), the other experiments were performed at material science department of Tampere University of Technology. The test materials were provided by SSAB.

According to the test results, none of the estimation programs are feasible for all steels. However, some certain programs can predict the HER for certain sheet steel with high accuracy, for example the program 6 for DX56D, which showed almost the same result as the test result. Based on the fracture and microstructure analysis, the ductility of sheet steels seems to be the main factor which affects the feasibility of an estimation program. Furthermore, the input selection of estimation program can also affect the estimation accuracy. According to the analysis, ultimate tensile strength (UTS) is a possible parameter which ensures the accuracy of estimation program.

PREFACE

This master thesis work was supported by SSAB Europe and especially M.Sc. Olli Oja. I should give great thanks to my examiner Associate Professor Pasi Peura for his comments and advices on my thesis. Great thanks also to my supervisor Mikko Hokka who always patient and helpful for my thesis work, and provided many ideas and guidance to me. Besides, I should also thank my colleagues who always help me when I met problems, and without their help, some experiments will be hard for me to finish by myself. I also need to thank my family which always support and encourage me to against difficulties.

Tampere, Feburary.2016

Shuai Chufan

CONTENTS

SYMBOLS AND ABBREVIATIONS

AHSS	Advanced high strength steel
ANN	Artificial neural network
CP	Complex phase
DP	Dual phase
DRMS	Digital recording and measurement system
FLD	Forming limit diagram
FEA	Finite element analysis
HER	Hole expansion ratio
HF	Hot-forming
IF	Interstitial free
MS	Martensitic steel
RA	Retained austenite
rpm	Revolution per minute
SEM	Scanning electron microscope
SAS	Self alignment system
TEL	Total elongation
TWIP	Twinning-induced plasticity
TRIP	Transformation induced plasticity
UTS	Ultimate tensile strength
UEL	Uniform elongation
UTS-UEL	Product of UTS and UEL
UTS-TEL	Product of UTS and TEL
YS	Yield strength
YR	Yield ratio

1. INTRODUCTION

Sheet steels have been applied in various industrial areas such as automotive, aircraft and building constructions due to its noteworthy merits, especially the outstanding formability. Meanwhile, hole expansion test is an effective mechanical test which always be utilized to characterize the flange formability of sheet steels. However, in order to obtain higher accuracy and reliable experimental data, large amount of repetitive tests are necessary which can cause increasing of the cost and reducing of the efficiency. In this case, estimation program is attracting more attentions to be as a verification or prediction method for the test results. As a result, the cost savings and accuracy of the test can be increased. [1-3]

The purpose of this thesis is to study and analyze the feasibility of several estimation programs. Theories on sheet steels, flangeability measurements, and artificial neural network (ANN) will be introduced first in this thesis. In the second Chapter, some common sheet steel grades and the application of sheet steels are introduced. In the third Chapter, introduction of parameters which related to formability, their measurements and influence factors of measurements are presented. After that, a Chapter of ANN in material research and the relation between tensile data and flangeability is introduced.

In the experiment part, a formable metal coated interstitial free (IF) sheet steel and four types of advanced high strength sheet steels are characterized by hole expansion test. The four types of advanced high strength steels (AHSS) include DP600, DP800, CP600 and CP800 where DP refer to dual phase steels and CP refer to complex phase steels. On the other hand, seven different hole expansion ratio (HER) estimation programs are selected to acquire a group of simulated HER values. All these programs are trained by using an ANN program called Generate44. Inputs of these estimation programs are derived from the tensile tests of the studied materials. In order to compare the microstructure and the fracture differences among selected materials, the fracture edges of hole expansion samples are studied by both optical and electrical microscope. Moreover, microstructures of selected sheet steels are studied by scanning electron microscope (SEM).

Final feasibilities of estimation programs are discussed by comparing the error ratios of each program. The analysis of feasibility is mainly focused on microstructure comparison and comparison between edge fractures of hole expansion samples. On the other hand, effect of program inputs selection and defects of ANN are further discussed in the discussion part.

2. SHEET STEELS

As a basic form in the metalworking industry, the application of sheet steels can be traced back to 1480 when the first rolling mill was designed, which used two cylindrical rollers to control the thickness of metals. Attributing to the low cost and excellent combination of strength and formability, sheet steel became widely applicable in the engineering field from the 18th centuries. Despite there are various small thickness steels such as plate or foil, however, the definition of a work piece to be considered as sheet steel should have a thickness range from 1.83 to 76.2 mm. Meanwhile, the thickness of sheet steels is often presented according to its gauge number, which the thickness of the work piece is increased with gauge number promotion. Some common sheet steels and relevant applications will be introduced in this Chapter. [4-6]

2.1 Common type of sheet steels

Most steels can be manufactured into sheet steels form by rolling. Various materials are manufactured into the sheet form in order to satisfy the different applications. In this section, some types of steels which are commonly used in sheet steel industry will be briefly introduced.

2.1.1 Advanced high strength steels

As the name implies, advanced high strength steels (AHSS) refer to the steels which provide excellent yield strength (>300 MPa) and tensile strength (>600MPa). As Figure 1 illustrates, AHSS can be categorized into several types. Among these different types of AHSS, dual phase (DP) and complex phase (CP) steels are two of the most common types of AHSS which have been utilized as sheet steels form. The high strength grades of AHSS sheet steels are appropriate for high strength and applications requiring formability. Meanwhile, attributing to the excellent energy absorption potential, AHSS sheet steels are usually used for safety applications in automotive industry. [7][8]

Microstructures of DP steels are mainly comprised by two phases. The hard phase is martensite and soft phase is ferrite matrix, which martensite provides high hardness and strength to the steel while ferrite ensures the steel with a good ductility and toughness [9]. In order to fulfill different application demands, the mechanical properties of the DP steels can be adjusted by changing the ratio between two phases. Various phase proportion can be achieved through different heat treatments. In general, DP sheet steels have low yield ratios (YR) and high strain hardening rates which are attributed to the combination of ferrite and martensite. [10] [11]

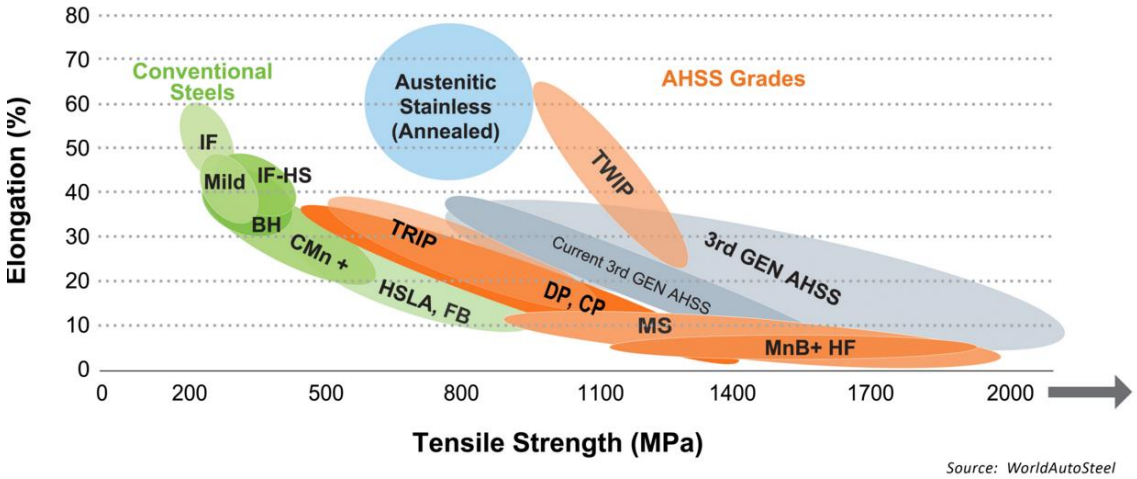

***Figure 1**.Mechanical properties of AHSS (red marked): transformation-induced plasticity (TRIP), dual-phase (DP), complex-phase (CP), twinning-induced plasticity (TWIP), martensitic steels (MS) and boron-based hot-forming steels (MnB+ HF). [12]*

Unlike DP steels, CP steels have more complicated microstructures which are typically comprised of martensite, bainite and limited amount of ferrite. Meanwhile, the volume of martensite in CP steel may be smaller than that of the same tensile strength DP steel. The biggest advantage of CP steels is fabricated good formability which attributes to fine structure and small hardness difference between diverse hard phases. In addition, CP steels always represent higher yield ratio and lower elongation when compared with the same tensile strength DP steel. [6][10]

2.1.2 IF steels

Interstitial free (IF) steels are also known as ultra-low carbon steels which provide excellent formability, deep drawing ability and no aging effect. Based on these properties, IF steels are ideal materials for the automobile industry. Generally, IF steels have high elongation and r value (> 40% and >2.0, respectively). [13]

A vital influential factor of IF steel is the content of free interstitial C and N. Large number of studies have revealed that the formation of {111} recrystallization textures in sheet steels has a positive effect on the deep drawing ability, i.e. a high r-value can provides better draw ability. However, free interstitial C and N atoms can lead to incoherent second phase precipitates such as titanium-carbides and aluminum-nitrides at grain boundaries of the grains, which are obstacles for {111} textures nucleation. Furthermore, free interstitial atoms can dramatically increase the aging effect of the steel which is harmful for deep drawing. Consequently, the content of free interstitial C and N has negative effect on the final formability of IF sheet steels. [14,15]

To avoid the effect of free interstitial C and N atoms, several micro alloying elements are added into IF sheet steels such as Ti and Nb which can stabilize the C and N as car-

bides and nitrides. However, both Ti and Nb are expensive for mass production, in order to reduce the cost of production, the original volume of C and N in IF steels are both lower than 40 ppm. Based on the low amount of C and N, the demand of Ti and Nb can be also decreased. In the industrial production, vacuum degassing is used as an approach to decrease the content of C and N. With low original content and alloying elements, almost all free interstitial C and N atoms can be eliminated from the basic ferrite matrix. Subsequently, {111} recrystallization textures can be formed to ensure there is no aging effect during the drawing process, as a result, the formability of IF sheet steels can be improved. [16]

2.1.3 Metal coated sheet steels

Except the bare AHSS and IF steels, metal coated AHSS and IF steels can also be manufactured as sheet steels. As Figure 2 illustrated, metal coated steels have a basic substrate steel with other metal coated on the surface. Commonly, the coating surface can be acquired by the following two methods. First is hot dip which immerses the steel in the melted coating metal to acquire the coating film. An example is the Galfan anti-corrosion coating which acquires by immersing steel in a 95% zinc bath with nearly 5% aluminum and other certain amount rare earth mischmetal[17]. Another method is electro galvanizing process which deposits the coating metal by electrolytic reactions such as the general zinc coating surface of sheet steels.[18]

In order to meet different application demands, various materials were chosen as the metallic coating and the substrate steel. For instance, Zn-Al-Mg alloy can be used as a corrosion resistance metal coating through hot-dip galvanized approach, while TiAlN was applied as an abrasive resistant metal coating by surface deposition.[19][20] Moreover, the formability and strength of metal coated sheet steels can be adjusted by using different coated metal in some specific situations.

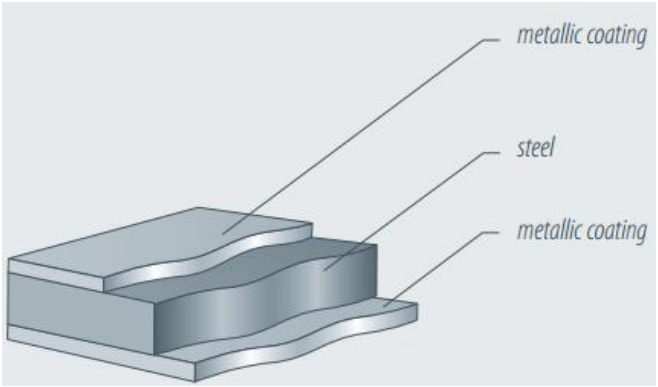

***Figure 2**.Schematic of metal coated sheet steel [21]*

2.2 Application of sheet steels

As a common material in our daily life, sheet steels have generated broad interest for using in manufacturing industry and construction fields. The good formability of sheet steel is suitable for manufacturing industry in order to get different shape work pieces. Meanwhile, high strength and durability of sheet steels can ensure the mechanical demand and sustainable improvement in the construction industry. Two main application fields of sheet steels will be introduced in this section, which provide basic information about the interests from the sheet steels.

2.2.1 Automobile industry

The automobile industry is the most important field which sheet steels are widely used in. In the 20^{th} centuries, the development of automobile industry has leaded to a great progress of the sheet steel forming technique. [3] In general, the materials applied in the automobile industry have to satisfy two requirements. The first requirement is relative low strength to weight rate, in order to reduce the weight of vehicles. Meanwhile, another point to consider is preferable strength and formability, which ensure the safety demand and convenient for manufacture. Sheet steel especially AHSS sheet steel is a good choice which can fulfill these requirements.

As Figure 3 shows, sheet steels always be used to fabricate the body panels and structural parts of the car. The light weight of the sheet steel can greatly reduce the fuel consumption thus increase the economic efficiency. On the other hand, high strength and formability of sheet steels provide the vehicle with a high energy absorption value which increases the safety and crash worthiness of the vehicle. Besides, the good formability of sheet steel makes it suitable for special shape components fabricating. [22-25]

Figure 3*.Application of sheet steels in Automobile application. [26]*

2.2.2 Construction market

In addition to vehicle fields, sheet steels are widely used in the construction market. For instance, sheet steels can be utilized to build the outer surface such as side walls and

roofing of buildings. Sheet steels have a profound history in the construction application, however, it became widespread in the 20th century because of the three main benefits as the following: cost effective, beautiful appearance and long life circle. [27]

Figure 4. (a) shows a house which the roof consists of sheet steels. As a construction material, sheet steels have both light weight and satisfied strength grades (usually up to 350 MPa yield strength), which improves the stability of the building. Moreover, the excellent formability of sheet steel enables the erection of building become more convenient. On the other hand, general roofing steels include additional protective coating which provides better corrosion resistance or other special abilities such as fire resistance or heat insulation properties for the building. Moreover, the sheet steels can be machined into different shape for the corresponding case. It can be an entire flat sheet steels or sometime be formed as corrugated shape as Figure 4. (b), which enhance the structure of the roof with the overlapping joints and low-pitch between each other. [28]

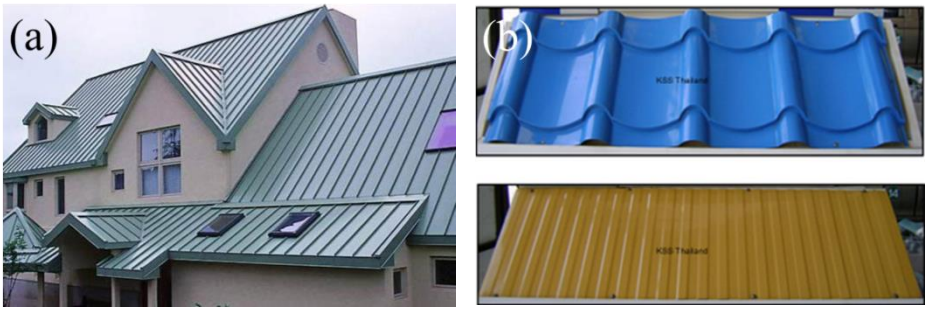

Figure 4.*Sheet steel application in buildings. A house with sheet steel roofing (a) two types of corrugation sheet steel (b) [29]*

With development of the architecture industry, material in nowadays construction field should not only satisfy the conventional mechanical demands of steels, but also be environmentally friendly. Carbon neutral steel building systems (CN-SBS) is a project which aims to improve the greenhouse gas emission from the construction industry. According to the research report of CN-SBS, the building industry provides around 30% greenhouse gas in the entire national emission amount of Canada each year. Some new sheet steel processing technologies have been provided to reduce the energy cost during the steel manufacturing process and increase the durability of the sheet steel. Therefore, the sheet steel in the future market should put more concentration in the environment field. [30]

3. FORMABILITY PARAMETERS OF SHEET STEELS AND RELEVANT MEASUREMENTS

Formability indicates the ability of sheet steel to undergo permanent plastic deformation without damage and/or failure. However, formability is a macroscopic conception to assess the material performance under all kinds of deformation circumstances. Thus, according to different plastic deformation and failure modes, specific parameters are used to represent the formability under certain circumstances.

In addition, an efficient and appropriate measurement is essential to determine a formability parameter in an accurate and convenient way. In Chapter 3, several parameters which related to formability and the corresponding effect factors will be introduced. Furthermore, two testing methods are also introduced after the parameter introduction.

3.1 Formability parameters of sheet steels

3.1.1 Tensile properties

Tensile properties are the most fundamental parameters for virtually all kinds of materials, which indicate the strength and ductility of sheet steels under a controlled tensile condition. The tensile test has a long history since the first systematic tensile test machine was designed by Petrus van Musschenbroek in the 18th century. After that, several scientists especially Thomas Young and George Rennie have improved the testing system. In nowadays, the standards and techniques of tensile test have become more mature, which have a highly efficient testing system with accurate testing output. [31]

Load-elongation curve is the direct result from tensile tests which usually translated as a stress-strain curve for further analysis. By analyzing the stress-strain curve, several tensile properties can be acquired and the ductility of sheet steel can be determined. These tensile properties are vital factors when considering the forming performance of a sheet steel. [32]

Tensile curves may have slight differences among different steels. Figure 5 presents two typical stress-strain curves. Apparently, the difference between them is that low carbon steel shows a fluctuation stage between elastic and plastic deformation stages. This fluctuation stage is called yield point elongation which affected by free interstitial atoms. For the material such as mild steel which has distinct yield point, the maximum and minimum stresses during the yield process are called upper and lower yield point, re-

spectively. While for some materials such as IF steel, the critical yield point is hard to be determined. Therefore, for this kind of ductile material, the yield strength point can be varied according to different measurement criteria. Generally the yield strength point is the point on the stress-strain curve which has 0.2% plastic strain. The measurement of yield strength (YS) will be presented in Chapter 6. The stress on the yield point is known as yield strength, meanwhile, the corresponding strain is yield strain.

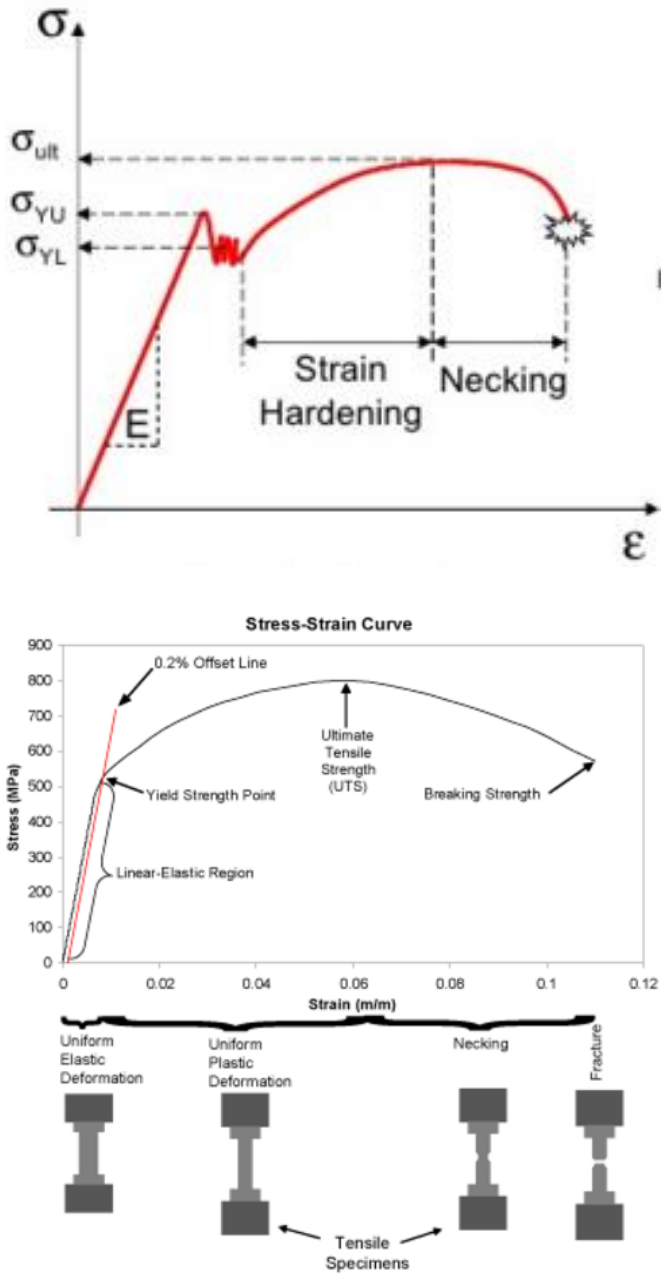

Figure 5. *Load-elongation curves of a low carbon steel (above) stress-strain curve of a ductile steel (below). [33, 34]*

Ultimate tensile strength (UTS) is the maximum stress value on the stress-strain curve, which refers the strength limitation of the material. The stress value on the peak point of

the tensile curve is UTS which is also the starting point of necking transition. After the peak stress, stress decreases with the increasing of strain and leads to the final fracture. While for some brittle steel, the UTS may be equal to the breaking strength since the brittle materials have no or little necking phenomenon.

The other parameter which is highly related to the formability of sheet steel is elongation. Elongation is the change in length of the extensimeter divided by the gauge length, which value is expressed as a percentage form and can be utilized to assess the formability of sheet steels under some normal forming processes such as rolling. For small elastic materials, the values of elongations are usually equal to the corresponding engineering strains. Generally, there are three important elongations on a tensile curve. The strain value at the ultimate tensile point is called uniform elongation while the strain value after that is called post-uniform elongation and the elongation value at fracture point is called total elongation. Unlike YS and UTS, elongation is not the internal character of sheet steel, which can vary according to the gauge length difference. The reason is that the plastic deformation of ductile materials is mainly concentrated in the necking area of the tensile sample. As a consequence, an extensimeter with smaller gauge length can measure larger localized strain. [35,36]

To characterize the forming property, n-value and r-value are utilized in the research of steels. During tension process, the correlation between strain and stress follows the Equation 1

$$\sigma = K\varepsilon^{n} \tag{1}$$

The σ represents the stress, ε refers to strain, K is the strength coefficient of the material and n is the n-value. The n-value usually approximately equals the strain at UTS, i.e. the initial point of necking. For sheet steels, n-value represents the uniform ability of the sheet steel during plastic deformation, which steel with higher n-value has better stretch forming performance. While r-value is the plastic strain ratio which calculated by Equation 2

$$r=\varepsilon_w/\varepsilon_t \tag{2}$$

The ε_w and ε_t are true strain on wide and thickness ranges, respectively. Generally, the r-value of steel refers the ability to resist thickness change during a tension or compression deformation. In industrial application, r-value has already been used as an indicator to estimate the deep drawing ability of sheet steel, which the higher r-value indicates better deep drawability.

3.1.2 Flangeability

As the previous segment mentioned, general formability of sheet steels can be determined from the tensile test, while in some large deformation and special shaping pro-

cesses such as stamping, hole-flanging or deep drawing, tensile properties are not enough to characterize the formability of materials. Figure 6 is the schematic of the stamping process which illustrates the deformation condition at the shear edge of steel sheets. As the figure shows, during the stretch flanging process, the cross thickness fracture occurs at the sheared edge of the sheet steel. To measure the steel formability under similar circumstance, flangeability is utilized as a parameter which indicates the difficulty that sheet steel can be made into a complex flanged shape in a fabricating process. [37-39]

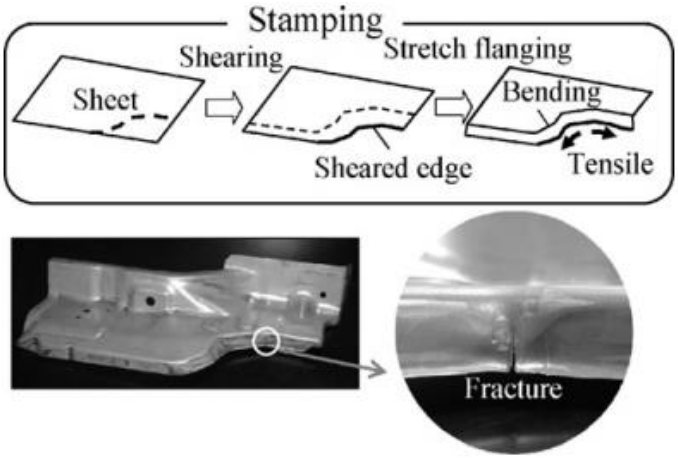

Figure 6.*Stamping procedure of 780 MPa high strength DP steel sheet and the fracture in stretch flanging. [40]*

3.2 Parameters effect on flangeability

During the past decades, many researchers have been discovered that flangeability can be affected by several factors. By controlling the effect parameters and changing the processing approaches, the formability of the sheet steel can be adjusted for different applications.

In addition, sheared edge condition which is affected by the previous machining process can also affect the flangeability of steel sheets. According to the research from Kenichiro et al., the unevenness and hardness of the sheared edge have negative effect on flangeability. [40] Furthermore, sheet steels with the burr at the edges always show worse flangeability than the steel with better edge condition. These kinds of external parameters can be improved by applying new advanced processing methods into the sheet steel fabrication. Such as use sharp tools for steel machining instead of worn tools. [43] Some external parameters such as blank hold force and punch location of the punching process can also affect the forming ability of the sheet steel.[41]

Except for the above external factors, it is well-known that microstructures can affect the formability of the steels as an internal factor. Several researchers have revealed that the larger amount of the soft phase in sheet steel, the better formability the sheet steel

can be acquired. For instance, the uniform of the microstructures and hardness among different phases are both principal factors for the flangeability. The research of Koh-ichi et al. revealed that excellent flangeability of sheet steels can be acquired with a uniform fine lath structure matrix and stable retained austenite (RA) films. [42] Thus, heat treatment and micro alloying are efficient methods in order to acquire excellent flangeability of sheet steels.

On the other hand, as a parameter which indicates the flangeability, the hole expansion ratio (HER) can increase with the improvement in the unity of the sheet steel microstructure. In this case, the unity of microstructures refers to two aspects, the phase diversity and the hardness difference between various phases. [43,44] Figure 7 illustrates the relationship between microstructure unity and HER. Apparently, bainite single phase microstructure provides higher HER than bainite multi-phase microstructure. An example is the IF steel with the ferrite single phase which is similar with bainite single phase always shows excellent edge flangeability compared with same grade CP steel. On the other hand, despite TRIP steel has much diverse phase composition than DP steel, the TRIP steel still shows better HER than DP steel. An explanation is the RA in TRIP steel which can transform to martensite thus decrease the hardness difference among various phases, as a result, HER of the TRIP steel is higher than DP steel. The research from Z.Z. Zhao et al. also indicated that RA can improve the compressive stress on the ferrite and bainite matrix to impede the crack propagations thus increase the edge flangeability of sheet steels. [24]

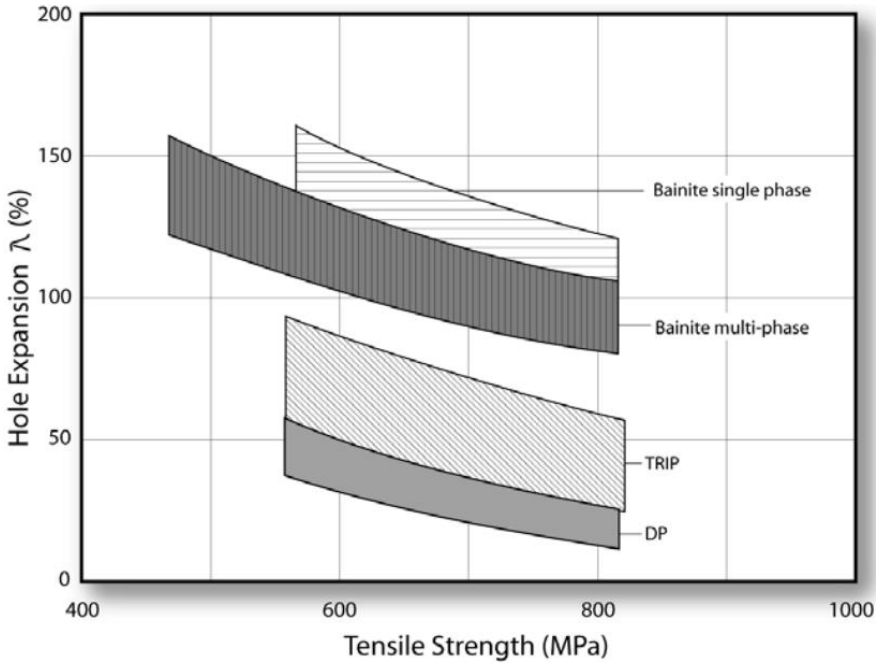

***Figure 7**.HER among several sheet steels with different microstructures. [43]*

3.3 Measurements of flangeability

3.3.1 Hole expansion test

The hole expansion test is the most common method which is used to measure the flangeability of sheet steels. The direct result of the hole expansion test is HER which the higher HER value represents the better flangeability. [45]

Based on ISO/TS 16630-2003, specimens for hole expansion are a thin plate sample with a punched hole in the middle of the sample. As Figure 8 illustrates, during the hole expansion test, the specimen is first fixed by the punching die. One thing need to be mentioned is that the center of the punching hole should be aligned with the puncher chip as much as possible to ensure the accuracy of the test.

The test can be started while all the parameters are set and the sample is fixed. During the test, a puncher with a conical head keeps moving with a constant speed to flange the hole in the sample until a cross thickness fracture can be seen at the edge of the hole, then the whole testing machine will be turned off and the puncher stop to stretch the hole. [37]

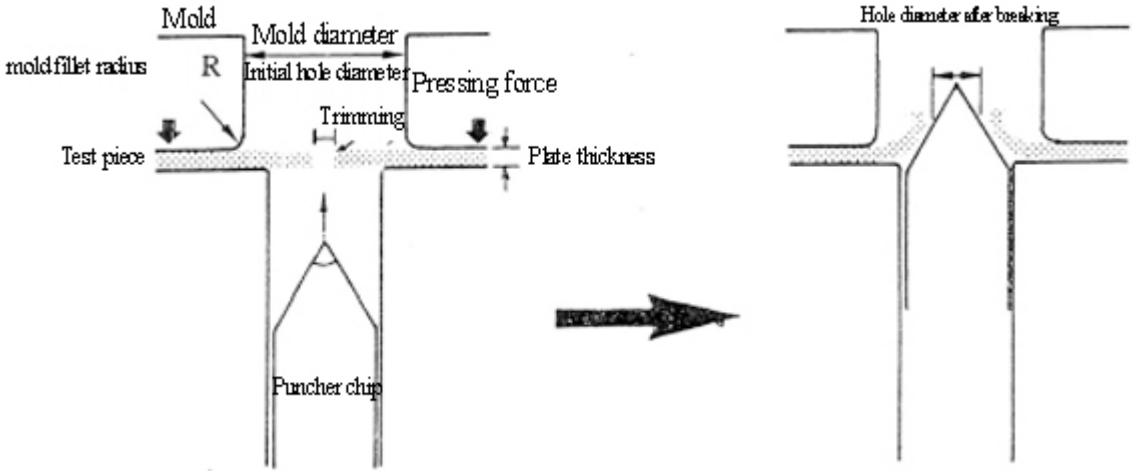

Figure 8 *Schematic of hole expansion test. [46]*

The hole diameter is measured before and after the punching procedure. Then, the HER value is calculated by the Equation 3 as follow:

$$HER = (D - d) / d \times 100\ [\%] \quad (3)$$

Where D represents the diameter of the punched hole after the test and d is the original hole diameter. [47]

3.3.2 Testing variabilities

As all the experiments, the result of the hole expansion test can be affected by both the absolute error from the measurement system and the personal error from the operational deviation. Therefore, results of the hole expansion tests may have differences even for the same specimen under the same test standard. Several influential factors and corresponding solutions are discussed in this section.

- **Blank holder**

The blank holder is the part of equipment for the hole expansion test, which is used to provide clamping force for fixing samples on a rigid position. The effect of the blank holder on the final HER result in some extent can be determined by the condition of the measurement. The research from Obermayer et al. demonstrated that the accuracy of the hole expansion test can be improved by using the elastic blank holder instead of the traditional normal sample holder. [41] One explanation is that the state of the deformations around the hole edge are not homogenous during the expansion process. The elastic blank holder can improve the forming conditions around the edge by adjust the stress and strain state at each point on the hole edge to enhance the reliability of the HER.

- **Penetration speed**

The penetration speed defines the raising speed of the puncher. According to the research of Chiriac et al., different penetration speed can lead to various hole expansion results even for the same material. [37] To be more specific, three different AHSS were studied in their research, and the result showed that with the increasing of the test speed, HER values of the steels were improved. However, the accuracy of the test cannot be unilaterial determined by the increasing of HER value.

- **Alignment**

As the Section 3.2.1 mentioned, the alignment between hole center and the puncher axis is a vital premise before the test start. Several reports have indicated that the HER value will decline with the increasing of offset value, especially for the high strength sheet steels. In other words, a well alignment device provides higher HER values. The reason is that a sample which is set with offset can aggravate the inhomogeneous condition at the hole edge, thus leads to an uneven plastic deformation phenomenon around the punching hole. As a result, the final outcome of the hole expansion test is not accurate.

One of the solutions to enhance the alignment of the test is to improve the testing system. For example, the Self Alignment System (SAS) is a system which can improve the alignment condition of the hole expansion test. The principle of SAS is to apply a preload on the specimen from the sample holder, which fixes the specimen under a loose

condition. After that, the conical puncher pushes the specimen slowly without any plastic deformation. Considering the specimen is on a loose condition, the sample is aligned with the puncher automatically when the puncher hit it. The next step is to remove the puncher and release the specimen fall back to the sample holder. Meanwhile, the sample holder fastens the sample with a higher clamping force. Then, the whole alignment process is completed thus the hole expansion test can perform with higher accuracy. [37]

- **Determination criteria of cross thickness fracture**

The effect of operator is also an important factor which can affect the test result. Considering the hole expansion test is stopped when any cross thickness fracture arises at the hole edge, so the determination criteria of the cross thickness fracture have huge influence on the HER values. In most cases, several cross thickness fractures appear simultaneously, which increase the difficulty of crack determination especially for naked eyes. As a consequence, the moment when the first cross thickness fracture arises is hard to determine accurately.

To optimize the accuracy of the hole expansion test, several improvements were invented. The digital record and measurement system (DRMS) has been proved as a good method which can effectively improve the accuracy of the cross thickness fracture determination. The principle of DRMS is to use a high speed camera for the image recording of the hole edges at each moment during the hole expansion test so that the edge condition on each second can be shown as a real-time image on the screen. After the test stop, each frame of the recorded images can be replayed again. The image of the first cross thickness fracture appearance can be selected from all the images. The next step is to use measurement software to characterize the hole diameter on the selected image for the final HER value calculation. [37] However, materials always have different extent elastic recovery which leads diameter differences between the final sample and the moment when the first crack appears, thus, the DRMS is only suitable for the steels which have small elastic recovery.

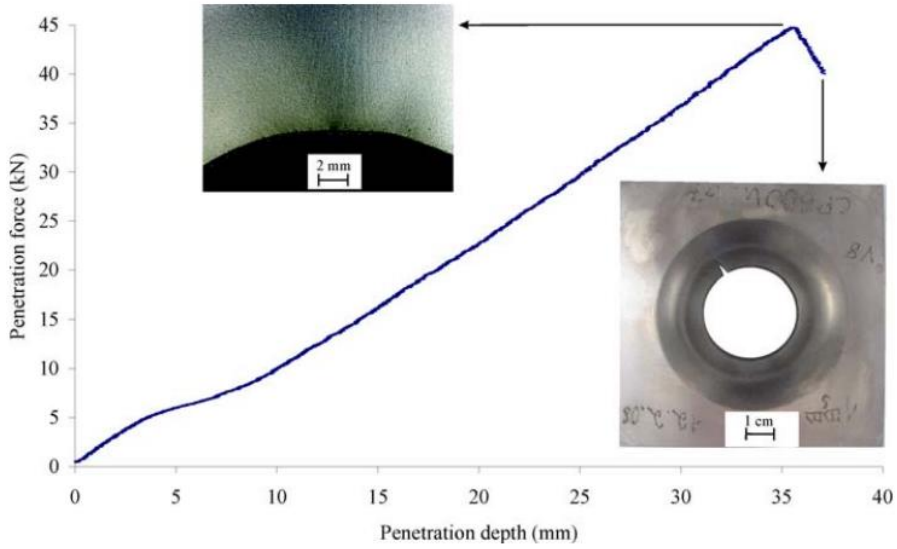

Figure 9*.Penetration force-displacement curve of CP600 sheet steel [48]*

Similarly, the method penetration force-depth diagram can also precisely acquire the first cross thickness fracture. As Figure 9 illustrates, it is a typical diagram to show the correlation between penetration depth and penetration force during the hole expansion test. Special camera and sensors are applied to monitor the required data for the diagram. After the test, the peak of the curve is determined to be the critical point when the first cross thickness fracture appears. Then, HER is calculated by using the diameter information at that point. [46]

3.3.3 Forming limit diagrams

The forming limit diagram (FLD) is another significant approach which is used to assess the forming behavior of sheet steel. The FLD is determined by repeating several formability experiments under different condition such as the hole expansion test. General the procedure to draw a FLD is introduced as the following.

First, the testing specimens are marked with meshes on the surface before perform the mechanical test, as Figure 10 illustrates. When a test is completed, the next step is to find the critical mesh circle which crossed by cracks or close to the fracture area and measure the diameter of the mesh circle in two orthogonal directions which along the meshes. Meanwhile, the original diameter of the circle is measured from a mesh circle which has no deformation. Furthermore, the major and minor strains at each critical point are calculated from Equation 4 and 5.

$$e_1 = (d_1 - d_0) / d_0 \times 100\% \quad (4)$$

$$e_2 = (d_2 - d_0) / d_0 \times 100\% \quad (5)$$

Where the e_1, e_2 refer to the major and minor engineering strains, d_1, d_2 refer to the diameters on major and minor strain directions and d_0 represents the original diameter of the mesh circle. If the strains in curve use the true strain values, the values are calculated from Equation 6 and 7

$$\varepsilon_1 = \ln\frac{d_1}{d_0} = \ln(1 + e_1) \tag{6}$$

$$\varepsilon_2 = \ln\frac{d_2}{d_0} = \ln(1 + e_2) \tag{7}$$

Where ε_1 and ε_2 represent the true strains on major and minor directions.

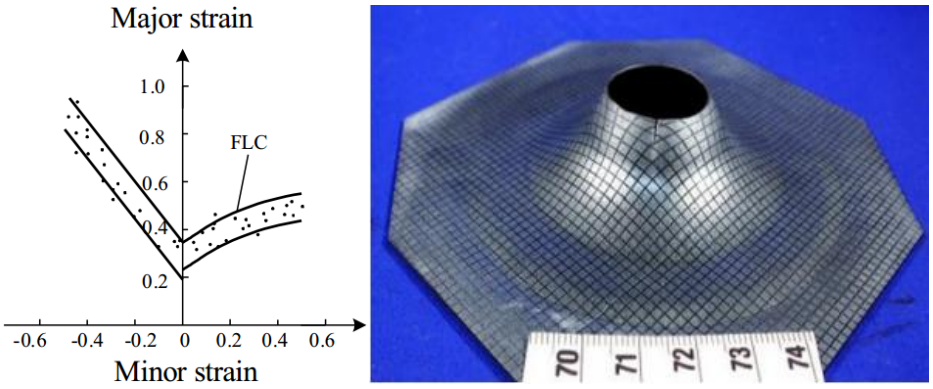

***Figure 10**. Example of FLD and the hole example specimen which applied for FLD analysis.* [49][50]

After the strain data under a certain circumstance determined, the test needs to be repeated several times under different sample shape or loading conditions. Groups of strain data under different conditions can be acquired after several repeating tests. With the groups of strain data, the FLD can be drawn as Figure 10. Considering the data on the curve are dispersive, there is a critical band in FLD which divide the curve into three parts. Large amount of tests demonstrated that, when the deformation area of a work piece is above the critical band, the material will have fractures. In the contrast, if the deformation area is below the critical band, fractures will not appear. Therefore, the fracture condition of sheet steel can be predicted by using FLD. Apparently, the FLD can only predict the deformation limitation of a material under certain strain condition. While the exactly mechanical properties such as HER can not be derived directly from FLD. However, the character of FLD still makes it always be used for some further estimation analysis such as finite element analysis (FEA). [51-53]

As an important analysis approach, the first FLD was proposed by Keeler and Backhofen in the year 1964 and Goodwin improved it at 1968. FLD is meaningful to sheet steel deformation analysis. If the FLD of specific type sheet steel is acquired, the strain condition of the sheet steel during a certain forming process can be predicted in advance, as a consequence, the failure of the work piece can be prevented. [54,55]

3.4 Estimation of Hole Expansion Ratio

Since the hole expansion test has several variabilities which affect the accuracy of the test, meanwhile, FLD cannot predict HER directly, some extra estimation methods have gained interests in the research field. An effective way to predict HER is to use some estimation programs which can estimate a test result by using some certain mechanical properties into empirical equations. Generally, the interior principles of estimation programs are some empirical equations as following [56, 69]:

$$\mathrm{HER} = 1.7\ (r_m)\ (e_{t(\%)})+15 \tag{8}$$

$$\mathrm{HER} = 478\ t + 2.56\ e_{t(\%)} + 35.3\ r_m - 58.2 \tag{9}$$

$$\mathrm{HER} = 85.7\ r_m - 31.4\ n_t - 23.6 \tag{10}$$

where *rm* and *nt* are r-value and n-value, respectively, *t* is the sample thickness, $e_{t(\%)}$ is the percent of transverse total elongation.

In this thesis study, some estimation programs are selected to estimate the HER by using tensile test data as the program inputs. The training method of estimation programs and relation between tensile data and HER will be introduced in the fourth Chapter.

All the estimation programs in this research are selected from the Materials Algorithms Project (MAP) Library. MAP is an online database which is created by the University of Cambridge and the National Physical Laboratory. MAP includes various modelling programs which can be employed in the materials science application.

As Figure 11 shows, according to the type of materials, MAP Library classifies all the resources into several categories, which are convenient for model searching. Besides the completed programs, some other relevant information such as subroutines and modules can also be found in this database. In addition, the programs in MAP can be written in any program languages. As a consequence, some special operation systems might be needed in some cases such as the Linux operating system.

After finding the appropriate programs, the executive programs and the source code can be downloaded in corresponding links. Some essential introductions and instances are illustrated under the program pages. Also the contact information of the author can be found in case there is necessary to contact the programmer.

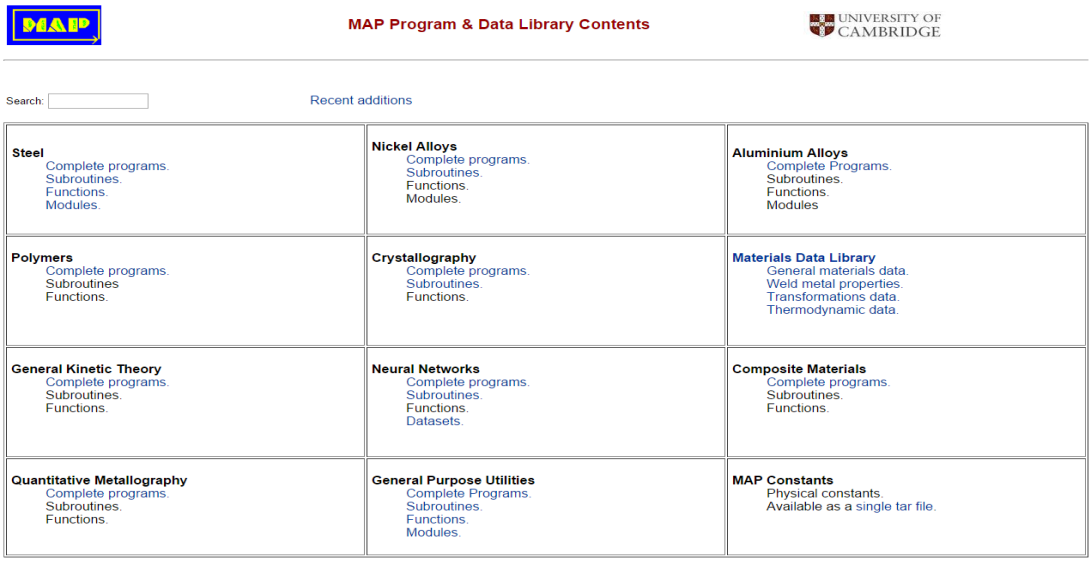

***Figure 11**.Interface of MAP Library [57]*

4. ARTIFICIAL NEURAL NETWORK IN MATERIALS SCIENCE

Modelling as an important method in theoretical study has been extensively used in materials science. In the research of material science, large amount of properties and phenomena have been revealed by massive experiments, some experiments results even show the qualitative correlation. For instance, the HER of C-Mn sheet steel is increasing with the tempering temperature rise in a range from 200^{o}C to 300^{o}C, however, the quantitative correlation between the temperature and the HER value is unknown. [52] In this case, a modelling analysis is necessary to show the result in a quantitative way, so that tempering temperature can be decided in a real industrial manufacture process. On the other hand, modelling can be used as a method which can predict some specific characters of a material. If the modelling result is highly precise, a modelling program can even replace a laboratory test in order to reduce the research cost.

An appropriate model should have the ability which can simulate a result by using several specific parameters as the model inputs. Meanwhile, the model should be feasible among a certain input range so that the similar case which input within the range can use this model to get the simulated result. A good example is the crystallographic theory of martensite which can predict the final phases from the original crystal structures. [58] For a model establishment, first, an empirical equation should be built. Then, the model needs to be verified with plenty of experimental data to correct and improve the equation of the model. Final step is to select the most feasible model which can be applied from a certain case to general conditions. [59]

Various methods and algorithms can be used to build a model in materials science research. Considering the estimation programs in this master thesis are trained by the artificial neural network (ANN) model with tensile data, the principle and applications of ANN, relevance between formability and tensile properties will be presented in this Chapter.

4.1 Principle of artificial neural network

The artificial neural network (ANN) is a type of machine learning arithmetic model which is inspired by the human brain learning and summarizing behavior. With an appropriate training process which uses large amount of experimental data, the neural network can summarize the statistics and find a regular pattern between several varia-

bles and the target result parameters or simplify a present empirical model. As a result, the correlation between those variables and the result can be determined. [60]

As Figure 12 illustrates, the structure of an artificial neural network can be categorized into input layers, hidden layers and output layers. The circles in the figure are called neuron, which input variables can export an output result by using a certain algorithm through the neuron. The data which is guided into the input layers serves as the input parameters (Xi in Figure 12) of the whole estimation program. After the processing of input layers, the outputs from the input layers will be selected as the inputs for the next layers, and the final model establishing is based on the regression of all these neurons processing procedures. Each layer includes an uncertain amount of neurons and the basic principle of it is similar to biology neural network which signals are processed through these neurons step by step. The final result of the whole ANN is achieved by this procedure and acts as the "cost" in Figure 12. [61]

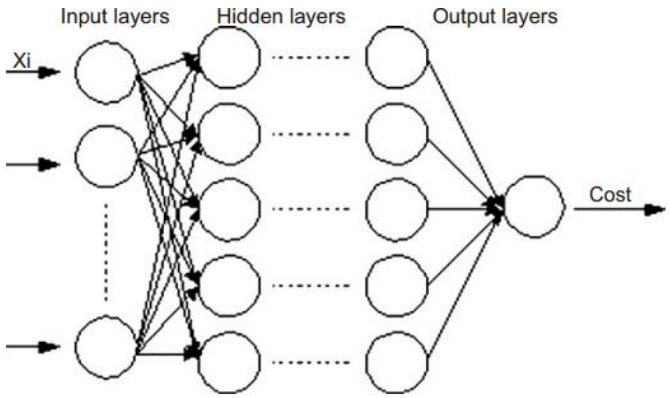

Figure 12.*Schematic of artificial neural network. [62]*

When training an ANN, the input and output of the ANN are both acquired from experimental data which input variables are selected experimental parameters and the corresponding output results can be checked directly from the experimental data. With several inputs and outputs data, the correlation equation can be built by neurons with linear fitting analysis. Based on this training mechanism, the accuracy of the final model can be improved by using large amount of training data. On the other hand, as the input between each neuron is randomly selected in a certain training case, the weight of each neuron in the final equation creation is different according to the contribution of each neuron to the final output of the whole ANN. [63] Once a modelling program is trained by ANN, it can be applied into the material research with several selected parameters to estimate the target parameter which is the output of the modelling program.

4.2 Relevance between Tensile Properties and formability

The estimation programs of HER in this thesis study are all using tensile properties as the model inputs. Therefore, the relevance between tensile properties and formability of sheet steels is introduced in this segment.

As a most common mechanical test, the tensile test is an effective way to acquire the basic mechanical properties of sheet steels. Since the tensile test is easy to perform and the testing process is controllable with high experimental accuracy, tensile data are suitable to be selected as the inputs of an estimation program.

According to Section 3.1, both ductility and flangeability are indexes which indicate the formability of sheet steel. Meanwhile, ductility and flangeability are characterized from tensile test and hole expansion test. As a consequence, an assumption can be proposed that the tensile data and hole expansion behavior of sheet steels have a close relationship.

In fact, large amount of researchers have discovered the qualitative relevance between tensile properties and hole expansion properties during the past decades. For example, elongation is derived from a tensile test, which shows corresponding deformation at each moment during the tensile process, and it can be acquired from the load-elongation curve directly. Hole expansion tests among various sheet steels demonstrated that under a same testing standard, a material which shows a higher elongation usually has higher HER values. [64-66]

As one of the parameters which can be obtained from a tensile test, strength also shows a strong relevance to HER. Considering HER is also an index which represents the ductility of sheet steel under specific plastic deformation condition, the relation between HER and strength of the sheet steel is in accordance with the trend of the ductility, which declines with the increasing of strength. Furthermore, the strength of the sheet steel is highly affected by the chemical component of the material. This is because alloy elements provide various microstructures and phases for the sheet steel. For instance, Fang et al. indicated that carbon content in C-Mn steel can strongly affect the HER of the material due to the carbide which is generated by carbon. With the increasing of carbon proportion, HER of C-Mn steel is decreased. Meanwhile, the hardness between harder and softer phases can also affect the HER values, which HER is decreased with the enlargement of hardness difference, and this is reflected as the changing of strength as well. [51][65][67]

According to the introduction in 3.2.1, both n-value and r-value are related to the formability of steel. Therefore, it has high possibility that n-value and r-value can affect the HER values. Kuo T Y et al. have demonstrated that the HER value is increased with the promotion of n-value and r-value. [63][65][66]

5. EXPERIMENTAL PROCEDURE

The experimental parts of this master thesis include the following four tests: hole expansion test, tensile test, microstructure analysis and fracture analysis. All the specimens for these tests were produced from SSAB Europe (Hämeenlinna). However, only the hole expansion test and part of tensile tests were carried on in the research centre in Hämeenlinna. Other experiments were all preceded in materials science department of Tampere University of Technology.

The details of the laboratory experiments include testing parameters, testing devices and testing procedure will be introduced in Chapter 5. Moreover, introductions of estimation programs for the hole expansion ratio estimation test are also presented in the following.

5.1 Materials

5.1.1 Compositions

Five different sheet steels were chosen in this study, and all of them were provided by SSAB Company. The steel grades of these sheet steels were DX56D, DP600, DP800, CP600 and CP800 steels. In these selected materials, DX56D was a formable zinc-coated interstitial free (IF) sheet steel, and other four steels were 600 MPa and 800 MPa grades dual phase (DP) and complex phase (CP) sheet steels, respectively. The main chemical components of these materials were listed in Table 1.

Table 1. *Nominal chemical compositions (w%) of selected sheet steels according to the standard: SFS-EN 10346*

Steel grade	**Main chemical compositions (%)**				
	C max.	Si max.	Mn max.	Cr+Mo max.	Nb+Ti max.
DX56D	0.12	0.50	0.60	0.02	0.30
DP600	0.17	0.80	2.20	1.00	0.15
CP600	0.18	0.80	2.20	1.00	0.15
DP800	0.18	0.80	2.50	1.00	0.15
CP800	0.25	0.80	2.20	1.20	0.15

5.1.2 Microstructures

Microstructure images under 500× and 5000× magnifications of these steels are presented in this section. Considering the microstructure of DX56D has much difference than other steels, an image under the 2000× magnification of DX56D is also presented.

Figure 13. (a) and (b) are images of CP800 microstructures. Vast quantity of hard phases such as bainite, retained austenite and martensite can be observed in Figure 13. (a). Furthermore, parts of the hard phases are aligned along a certain direction which demonstrates the microstructural banding in CP800. On the other hand, the grain boundaries are hard to distinguish with 500× magnification as Figure 13. (a) shows. However, grain boundaries can be identified with higher magnification as Figure 13. (b).

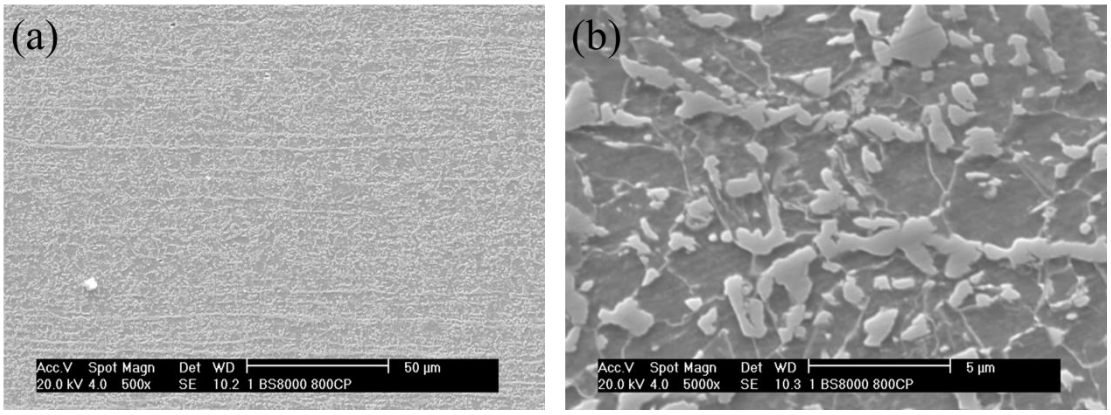

Figure 13*.SEM images of CP800 under different magnifications.*

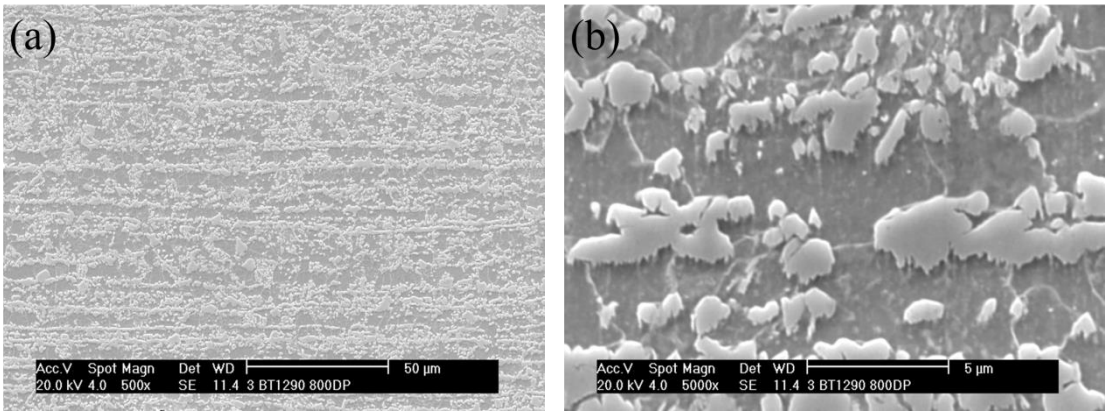

Figure 14.*SEM images of DP800 under different magnifications.*

Similarly, the microstructure of DP800 steel also contains a lot of hard phases and alignment as Figure 14 illustrates. The difference is the less diversity of hard phases and the amount of second phases is smaller than CP800 steel. Martensites are the main content of these hard phases, the rest phases are small amount of bainite. Moreover, the

microstructural banding phenomenon in DP800 is more apparent. Furthermore, there are less hard phases and grain boundaries appear in Figure 14. (b). In addition, the edges of those hard phases have some fluctuation and sharp edges which directions of those edges are the same.

For CP600 steel, despite hard phases still show the microstructural banding tendency, but on the whole image aspect, hard phases are more disorder than 800 MPa grade steels. In Figure 15. (b), an apparent difference with 800 MPa grade steel is that CP600 steel contains significant less martensite. Similarly, grain boundaries of CP600 in one visual field are less than 800 MPa grade steels. One possible result can be estimated is that the grain size of CP600 is larger than the previous two steels. Different with CP800 steel, the edges of hard phases in CP600 show some fluctuation along a certain direction, but those edges are smoother than edges of hard phases in DP800 steel.

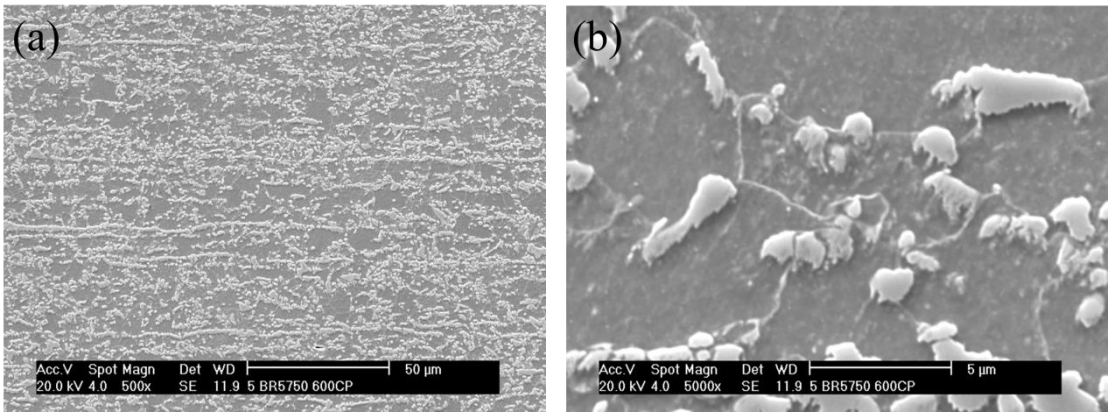

Figure 15.*SEM images of CP600 under different magnifications.*

Generally, the microstructure of DP600 is similar with CP600 which also has large grain particles with second phases disperse in the basic ferrite matrix. The difference is that DP600 steel has a larger density of hard phases. In Figure 16. (b), the edges of hard phases are sharper and point in diverse directions when it compared with CP600 steel.

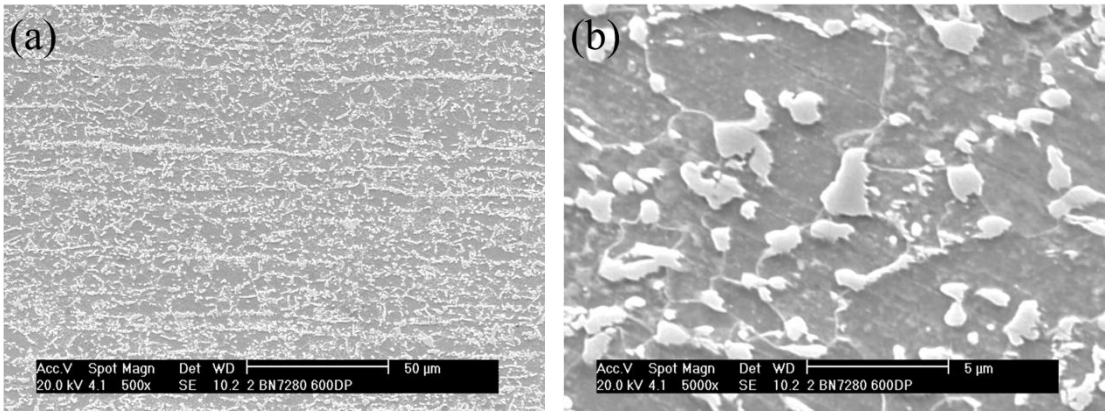

Figure 16.*SEM images of DP600 under different magnifications.*

Compared with the above steels, DX56D steel shows totally different microstructure as Figure 17 illustrates. As a single ferrite phase alloy, first, there are no hard phases appear among different grain particles. Second, only parts of the grain particles have internal hard structures and those structures have better and clear alignment than the previous steels. Meanwhile, these hard structures are mainly consisted by stabilized carbides and nitrides which are different structures than AHSS. Last, the grain particles are much larger than other steels while carbides and nitrides inside the grains are smaller than hard phases in other AHSS steels. This type of microstructures are mainly contributed by the formation of {111} texture during the recrystallization process.

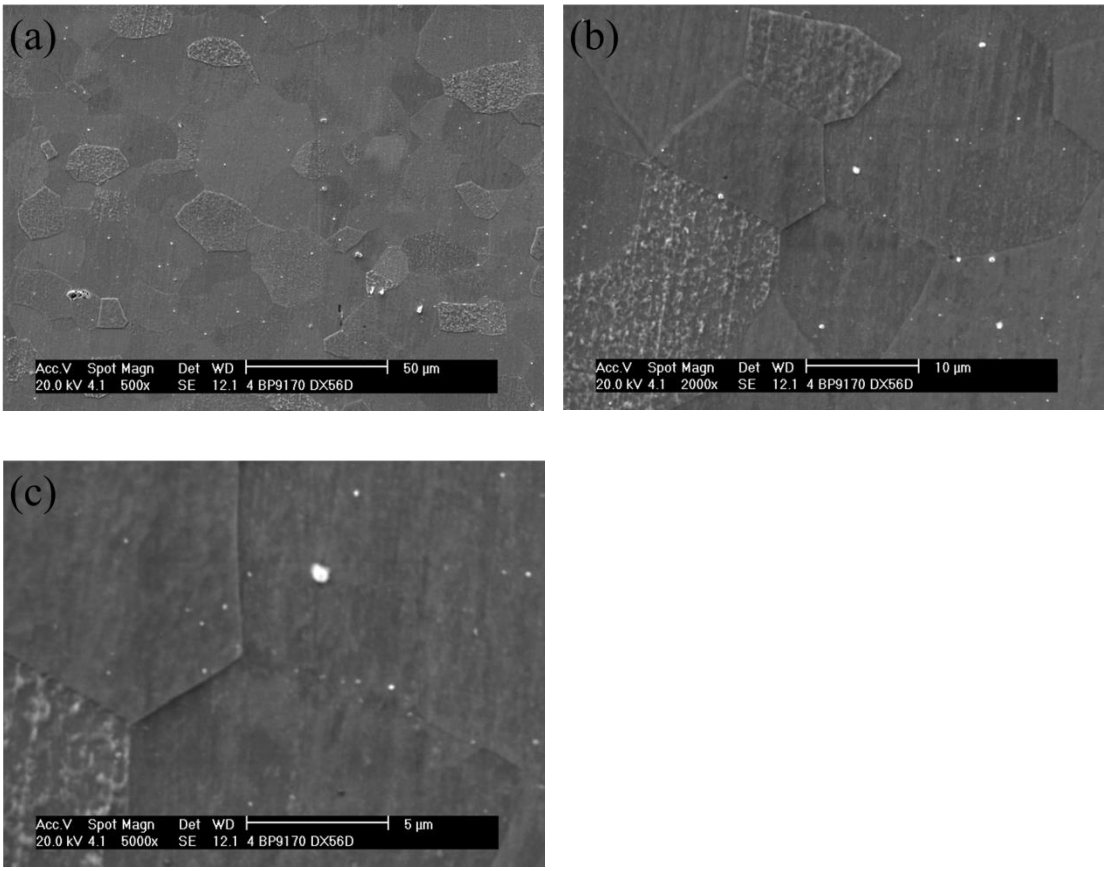

Figure 17.*SEM images of DX56D under different magnifications.*

5.2 Tensile test

The tensile test was performed in this research work, which aims to acquire the tensile properties of each material as inputs to the program estimations. Considering that sheet steel has anisotropy character, each material should take tensile test on rolling direction, transverse direction and 45 ° from the rolling directions, respectively. Tensile tests on rolling and transverse directions have already done in SSAB Company. Consequently, the experiments which are introduced in this section were performed in department of materials science of Tampere University of Technology and the microstructures samples

in the tensile tests were taken from sheet steels along 45 ° directions according to ISO 6892-1:2009 standard.

5.2.1 Specimens and Test Device

All the tensile test specimens were machined from the end of the sheet steel coil with longitudinal axis inclined with 45^{o} to the rolling direction. Compared with the front and middle part of the sheet steel coil, the end of a coil has better ductility. This is because the end of a steel coil reaches the cooling unit late during the cooling process of sheet steel. Testing samples were prepared with the same length and width, and the precise dimension is illustrated in Figure 18.

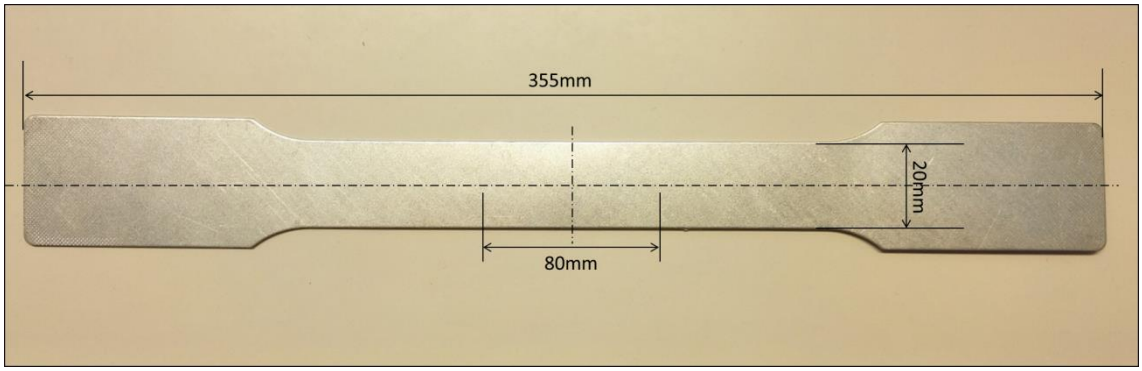

Figure 18.*Specimen of the tensile test along 45 ° direction from the rolling direction*

The testing system of the tensile test was Instron 8800 servohydraulic testing system as Figure 19 shows. Both dynamic static and static testing can be applied with this testing system and the axial force capacity of the system is ± 100 kN. Two gauges with gage length 80mm were applied in the tensile tests which are used to measure the dimension change of the samples in both length direction and transverse direction.

The whole tensile test was controlled by the connected computer with corresponding controlling software. Besides setting the experimental parameters, the software can also present the following four different real-time curves during the experiment process. These real-time curves are Load-time curve, position-time curve, load-strain curve and load-position curve, where the load refers to the tension load value, time refers to experiment time and position refers to the instant gauge position compared with the original position.

Figure 19.*Instron 8801 servohydraulic tensile machine and the grip. [68]*

5.2.2 Experiment Procedure

Despite all the specimens were machined with the same dimension, the thicknesses of samples between different materials were various due to the different thicknesses of original sheet steels and the operating deviation in the machining process. In order to improve the accuracy of the test, all the specimens were measured manually before set on to the experimental devices.

Samples can be fixed on the tensile machine after dimension measuring. Two extensometers were attached along the length direction and width direction, respectively, which were used to measure the dimension changes on these two directions.

The next step was to set the experimental parameters into the controlling computer program. The testing temperature was room temperature and tension piston movement kept constant during the whole test. Furthermore, all the strain values were balanced before the test started.

The tensile test was stopped after sample breaks. Meanwhile, test results were presented in Excel format which represents position, load, strain values on each time point. Once the experimental data saved, the broken sample was released and gauges were detached.

To maximize the accuracy of tensile strength, each material took three parallel experiments and the final value of each mechanical property was the average value which derived from those three parallel tests.

5.3 Hole Expansion Test

The hole expansion test as the main experiment in this thesis research, the principles and affection factors of it has already been introduced in Chapter 3. The main purpose of the hole expansion test in this research is to acquire the testing data of the hole expansion test for comparison with simulated HER values. Testing device and samples of the hole expansion test are presented in this section.

5.3.1 Specimens and Test Device

The same with tensile test samples, specimens for the hole expansion test were also taken from the end of the sheet steel coil. Considering the specimens were taken from the same area on the sheet steel, the effect of the mechanical variety between different part in sheet steel can be minimized.

Research of R.J. Comstock et al. revealed that the HER increase with an increase in the thickness of test samples. [69] However, because of the thickness limitation of different sheet steels, the thickness of each sample was various. For sheet steel which has better ductility such as DX56D, DP600 and CP600 steels, the sample thickness were 1 mm. While for higher strength grade sheet steel DP800 and CP800, the sample thicknesses were 1.5 mm and 1.3 mm, respectively. Despite the thickness of each sample was different, according to ISO/TS 16630-2003 standard, the hole size and the length of side was the same. As Figure 20 illustrated, all the specimens were machined into a square shape which length and width were 107 mm with a 10 mm punching hole at the center of each sample.

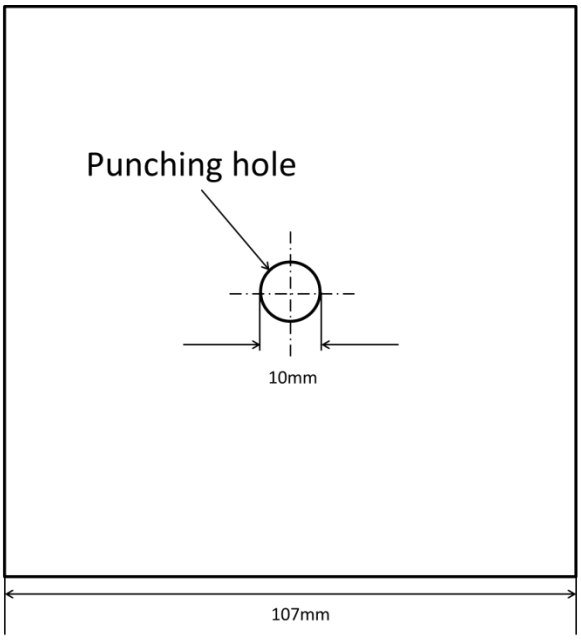

Figure 20*.Schematic of the hole expansion sample and dimensions.*

Erichsen 142-40 testing machine was chosen to carry the hole expansion test. It is a machine which is designed for several mechanical tests of sheet steels, such as the hole expansion test and deep drawing test. The machine is electro-hydralic drive with maximum 400 kN drawing force, and maximum 220 kN blank holder pressure. In addition, a video camera was fixed above the punching hole which was utilized to observe the hole expansion condition from the vertical side. The output of the video camera was displayed on a connected monitor screen which showed the real-time images of the test.

5.3.2 Experiment Procedure

Considering there were some operation deviations during the machining process, the diameter of the punching hole was measured again before each specimen set into the testing chamber. In order to improve the accuracy of the test, each hole was measured in two different directions and the final value of the diameter was the average value of those two values. One thing should be emphasis is that the center of the punching hole should align with the center of the puncher so that the punching condition at each point on the hole edge was the same. Meanwhile, to eliminate the effect from burrs, the conical puncher punched the hole from the opposite side of the surface which contains burrs at the hole edge, thus, there is no contact between burr and conical puncher during the hole expansion process. The whole test was taken under the room temperature condition. After the specimen fixed and the testing chamber closed, press the corresponding bottom to clamp the sample. The pressure for the sample clamping was a fixed value which was 50 kN and the moving speed of the puncher was 15 mm/min.

Hole expansion test started after all the parameters was set down and the sample fixed. As Figure 21 shows, there were four main windows on the control panel of the testing machine which displayed punching location, punching force, clamping force and punching speed, respectively. The clamping force and punching speed kept constant during the hole testing process while the punching location and punching force were increased during the process. It is because the punching location indicates the location of the puncher which value was 0 at the beginning and increased steady with the movement of the puncher. Similarly, for punching force value which needs larger load to continue the punching process, as a result, the value was also increased during the experimental procedure. The test was ended by pressing the stop bottom on the control panel once the cross-thickness fractures appeared on the monitor screen.

After the test, the final diameter of the punching hole was measured for the hole expansion ratio calculation. The diameter of the punch hole after the test was also measured on two different directions, and the final value of the hole diameter was the average values of these two diameters. On the other hand, three parallel experiments were taken for each material in order to minimize the experiment deviations. The final HER value was determined by calculating the average value of the three parallel experiments results for each material.

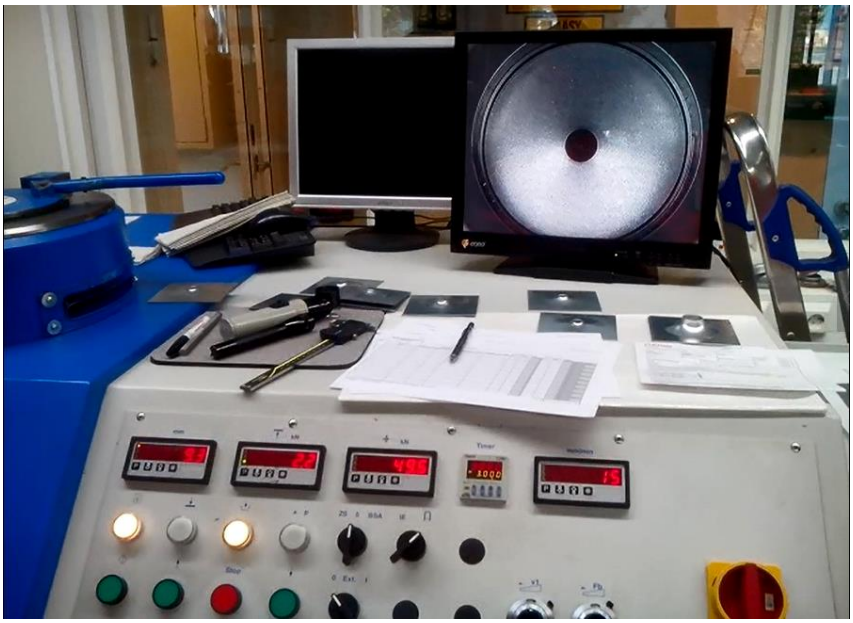

Figure 21*.Control panel and the monitor screen during the hole expansion test process.*

5.4 Estimation of hole expansion ratio

Another important part of this research is the program estimation of HER. After the hole expansion test completed, the testing result should compare with the predicted results for further analysis. Several estimation programs were chosen to calculate the HER. The database of algorithmic programs already introduced in Section 3.4 and the selected estimation programs will be introduced in Section 5.4.

5.4.1 Estimation programs

Estimation programs which applied in this thesis have been programmed by S Chatterjee from University of Cambridge in December 2006. In the estimation work, seven different programs with various input parameters were applied. The inputs of those programs are listed as the following:

Inputs parameters of Program 1: Yield strength (YS), Ultimate tensile strength (UTS), Yield ratio (YR), Uniform elongation (UEL), Product of UTS and UEL (UTS-UEL)
Inputs parameters of Program 2: UTS, UEL
Inputs parameters of Program 3: YS, UEL
Inputs parameters of Program 4: YS, UTS, YR, Total elongation (TEL), Product of UTS and TEL (UTS-TEL)
Inputs parameters of Program 5: UTS, TEL
Inputs parameters of Program 6: UTS, UTS-TEL
Inputs parameters of Program 7: UTS-TEL

All the programs have already been trained by an ANN called Generate44. Consequently, estimation programs can generate simulated results directly without any additional training processes. Considering the different relevance level between those mechanical indexes and HER, final HER values of prediction programs can be various. Thus by comparing the differences among each simulated result, the optimal prediction program for a certain material can be chosen.

Those programs had two different type versions which can run under PC or LINUX operation systems. Meanwhile, the details of the programs might have slight difference within these two versions. While in this research work, all the programs were performed under PC operation system.

5.4.2 Modelling process

The data of input parameters were acquired from tensile tests which already be introduced in Section 5.2. Considering that sheet steels might have anisotropic property, each material had three groups of prediction tests, which used the tensile data on transverse, rolling and 45^{o} from the rolling directions as the program inputs. Estimation tests started after all the demand inputs acquired and the procedure is introduced as the following.

First, all the tensile data should be tapped into a DAT file named *test* which is the file of estimation program inputs. After inputs fixed, the program can execute by clicking the executive program named *model*. One thing need to be emphasized is that the format of parameters in the test file should correspond with the format in the example of the program in MAP, otherwise, the program will be terminated.

If the program runs smoothly, the program windows will display each ongoing stage through the estimation process. After the estimation process finish, the result can be checked in the *model_result* DAT file. In the result file, the first line of values was predicted HER, and followed by a line of sigma modelling uncertainties which had no effect on this research. There was also file named *error_mess* which can be used to check if there were any error occurs during the estimation process.

5.5 Microscopy

The research part of this thesis work is to analyze the factors which cause the difference between testing results and predicted tested results. Considering that different materials have different microstructures and the fracture mechanisms, optical and electron microscopes are essential to analyze the difference from these two aspects. Testing devices and sample preparation processes are introduced in Section 5.5.

5.5.1 Optical microscope

In this research, the optical microscope was chosen to study the cross thickness fractures of the hole expansion samples on a low magnification level for the crack analysis. The optical microscope used in this work was Leica MZ75 stereomicroscope. As a stereomicroscope, it has two eye pieces which can increase the accuracy of the image by adjusting the images from each eye pieces. As Figure 22 shows, MZ75 has two adjustable light sources, which illumination directions are changeable. The whole microscope was controlled by the attached computer which can set parameters and make labels on images. By using the controlling software in the computer, fractures can also be observed on the computer screen.

***Figure 22**.Leica MZ75 stereomicroscope*

In this research, zoom drive parameter for all samples were 1.00 ×while the main objective magnifications were 2.0 ×or 0.5 ×according to different samples. The fractures can be clearly seen from the eye lens or the computer screen after all the adjustments completed. Meanwhile, fracture images were saved with the controlling software. The crack size was directly measured from the images by using the control software, and the scale bar was also added on the image before the image saving.

5.5.2 Scanning electron microscope

The scanning electron microscope was applied for the microstructure analysis of each sheet steel and the fracture analysis of hole expansion samples. Philips XL-30 SEM was chosen for microstructure observations. Figure 23 is the configuration of Philips XL-30 SEM.

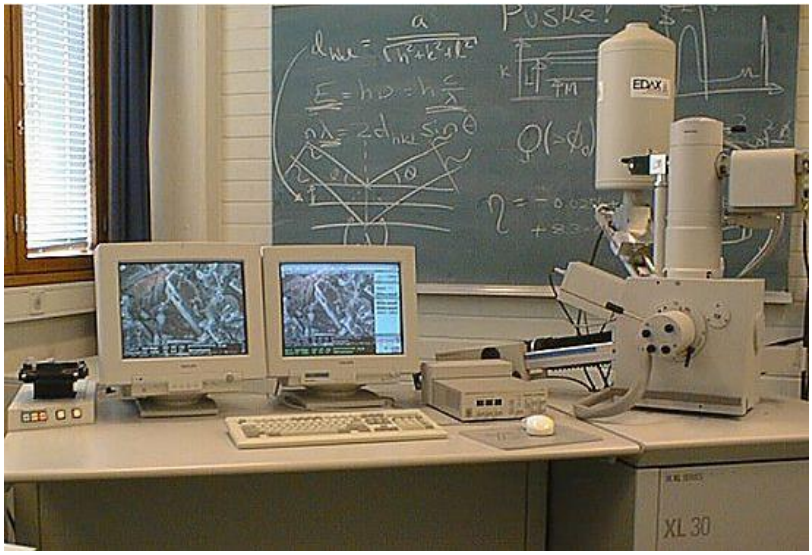

Figure 23.*Philips XL30 scanning electron microscope and the control computer unit. [70]*

Compared with the optical microscope, XL-30 has higher magnification which can reveal more details of the sample. Moreover, the depth of field is deeper than optical scope. In addition, SEM sample preparation is easier than a transmission electron microscope sample preparation, and the scanning speed of XL-30 is faster than other electron microscopes.

All the samples were cleaned by ultrasonic cleaning before set into the observation chamber. The samples were immersed in 16^{o}C technical ethanol solutions to do the ultrasonic cleaning for 3 min. After that, the observation surface was washed by ethanol again and a blower was used to dry the sample. Once the sample cleaned, it can be fixed into the chamber of SEM. XL-30. SEM. XL-30 has a sample holder which can fix several samples at one time, as a consequence, the chamber has no need to open frequently for the sample changing. Before the test, the observation chamber was vacuumed for scanning. When the observation completed, all the data and images were saved by the controlling computer unit.

5.5.3 Sample preparation

The surface of the sample for microstructure study needs special treatment before observation under the electron microscope. However, in the fracture observation experiment, the original dimension of the sample was too large to set into the observation chamber of the electron microscope. To solve these problems, all the samples were prepared by several processes before set into the SEM chamber. Operation processes of the sample preparation and testing devices are introduced in this Segment.

- **Cutting**

Cutting was the first process of sample preparation which cut the large sample into small pieces to fit the dimension demand of SEM. In this research, samples of microstructure and fracture observation were both machined with the cutting machine Struers discotom-5. This cutting machine is appropriate for small sample cutting and it can move the sample stage either in manual or automatic way during the cutting process. Furthermore, the cutting plate is changeable according to different hardness samples. In this test, 60A25 cutting plate was chosen for the sample cutting. Meanwhile, speed of sample stage remained 0.2 mm/s under the automatic moving mode. The cooling liquid was irrigating the sample automatically during the cutting process in order to keep the whole process under the room temperature condition.

Samples for the microstructure and the fracture observation were taken from different part of the steel. As Figure 24 illustrates, samples for the fracture observation were prepared from the specimen after the hole expansion test. In the image, the black lines denote the cutting lines. Meanwhile, the parts which are covered by red dashed line denote the area where the sample was taken. One thing should be emphasized here is that the sample area should have at least one cross thickness fracture. After the sample cutting, a mark was carved on the backside of the sample which indicated the rolling direction of that sample for the further fracture analysis. There were no other special treatments for the fracture observation samples, the samples can directly set into SEM chamber for further analysis after cutting.

Unlike fracture analysis samples, the microstructure observation samples were prepared from the tensile test specimens. Figure 25 indicates the sample area of the microstructure samples which were machined at the gripping head of the tensile test specimen. It is worth noting that the observation surface of the microstructure was the cross section area of the tensile test specimen. It is because the surface of the sheet steel might have some special surface treatment such as the zinc coating of DX56D which can affect the surface microstructure analysis.

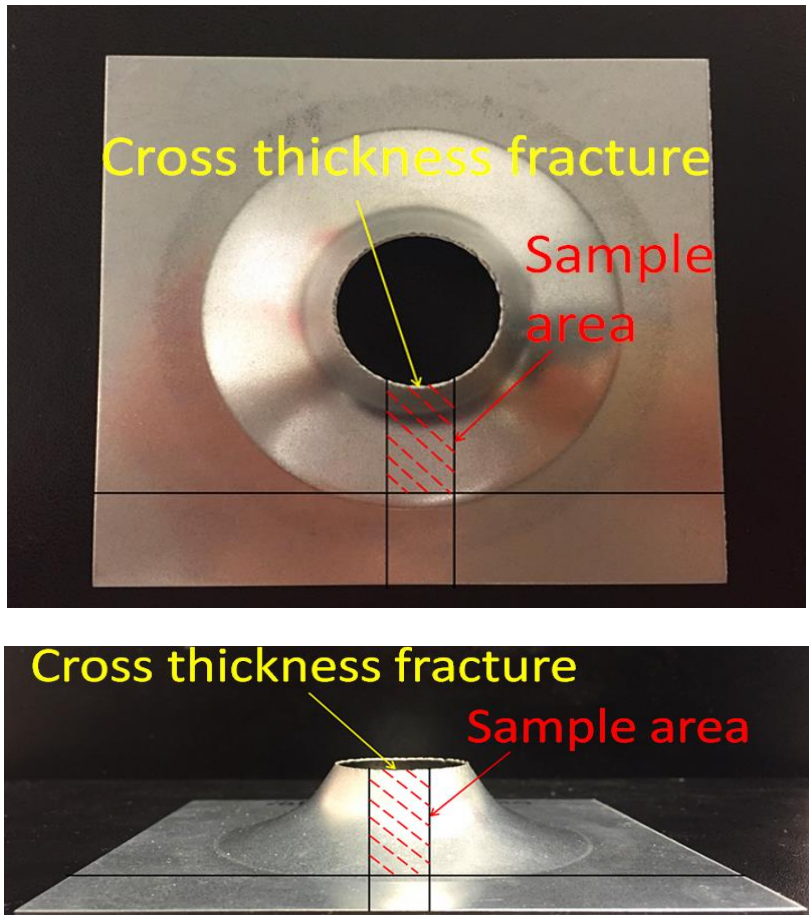

Figure 24.*Schematics of the sample area on the hole expansion specimen for fracture observation. Upper image is the schematic on vertical view and bottom image on lateral view.*

Figure 25.*Schematics of the sample area on the tensile specimen for microstructure observation*

- **Further preparation for microstructure analysis**

Considering the cross section area of the tensile test specimen was too narrow, all the samples for microstructure analysis were immersed in a small ingot which can hold the sample and stand on a horizontal plane. As a result, the cross section area can be ob-

served from the vertical side. In this thesis, samples were fixed in a ingot through hot resin method, which is quicker than cold resin and has no effect on microstructures of steels. The resin machine for this stage was the Struers Cito Press-10 hot resin machine.

The following steps were grinding and polishing which aim to improve the surface condition of the specimen. The device for grinding was BUEHLER Phoenix 4000 grinding machine and the rotating speed of the grinding plate was 150 rpm. Meanwhile, roughness of sandpaper was gradually decreased during grinding from P120, P320, P600 to P800 and P1200.

The Pedemax-2 polishing machine was utilized for the polishing process, which rotating speed was 200 rpm. During the polishing process, a special diamond liquid was added to polish the surface. 3 um diamond liquid was applied at the beginning of the polishing for rough abrasive and 1 um diamond liquid was applied at the end of the polishing process to polish the surface on a smaller scale.

Furthermore, 4% nital solvent was used for the etching process. The etching time was various, which depended on steel types. For DP600, CP600 and DP800 steels, the etching process only took 2 seconds, while 4 seconds and 5 seconds were essential for DX56D and CP800 steels, respectively. Moreover, a further step to emphasize is that the sample surface was roughly observed under an optical microscope to ensure the surface was etched with an appropriate condition. Some previous preparing steps were retaken for some over etched samples.

After all the above processes, the sample preparation for the microstructure analysis was completed, and the final sample was presented as Figure 26 illustrates.

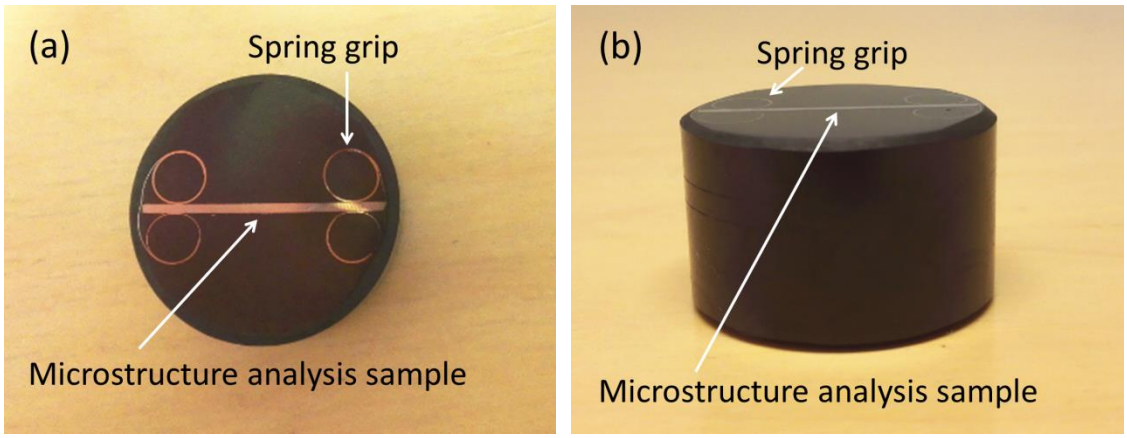

Figure 26.*Final sample of the microstructure analysis. (a)vertical view (b)lateral view*

6. RESULTS

Large amount of measurements, experiments and calculations were taken during the research process. Results are classified according to different experiments and will be presented in Chapter 6 with a brief introduction and explanations. Except original test results, feasibility comparisons of estimation programs are also be illustrated in Chapter 6. Majority result data are the original data which are derived directly from experiments. While some average values and special calculated results will be mentioned separately. Further analysis and discussions will be presented in Chapter 7.

6.1 Tensile test

The tensile test results are first introduced in this Section. In this research, each material which applied in the tensile test had three parallel tests. However, some tests results were invalid due to cracks appeared outside the extensimeter measurement parts so that strain data under this circumstance cannot be collected accurately. As a consequence, only valid typical test results will be introduced.

6.1.1 Stress-Strain Curve

The output of the tensile test was not strain-stress curve directly. As we mentioned in 5.2, during the tensile test process, four types of real-time curves were presented. After the tensile test finished, those four curves were translated and integrated as an Excel document. With the output data, the load and strain of the gauges on each time point can be checked afterwards.

However, the load-strain curve is not the final stress-strain curve. To interpret the direct output into the stress-strain curve, some equations are essential as Equation 11:

$$\sigma = \frac{F}{A_0} \tag{11}$$

Where σ is the engineering stress, F is the loading force and A_0 is the original cross section area of the sample. The value of the loading force at each time point was acquired directly from the output data sheet, and A_0 were calculated from width multiplies the thickness of each sample. [71]

On the other hand, the strain in the output document is the strain of gauges. Equation 12 was applied to transfer the strain of gauge into the strain of sample:

$$\varepsilon = \frac{\Delta l}{l_g} \tag{12}$$

Where ε is the strain of the sample and Δl is the strain of gauge and l_g is gauge length. Considering elongations for estimations were both presented in percentages. The ε values in final stress-strain curves were multiplied by 100.

All the input parameters which were used in the estimation programs were the engineering stress and strain value, so there is no need to do further calculation for true stress and strain. After the engineering stress and strain calculated, the stress strain curves were acquired.

Figure 27 is the typical integrated testing results of the stress-strain curve along the rolling direction. It is clearly that the yield strength (YS) of DP steels are lower than the same level CP steels, which CP800 and CP600 steels have 582 MPa and 441 MPa YS, but DP800 and CP800 only have 516 MPa and 366 MPa respectively. Furthermore, DX56D steel shows the lowest YS with only 144 MPa. Moreover, all the steels have really small elastic plastic deformations and no distinct yield points, which demonstrate the low content of free interstitial carbon and nitride of these steels. Therefore, the elongation values of these steels are approximately equal to the corresponding strain values.

Unlike the YS, the uniform elongations (UEL) and total elongations (TEL) are various among different steels. First comes to the DX56D steel which shows the best ductility with 42% TEL, and the UEL of DX56D is nearly the same as the TEL of CP600 steel which TEL value is 20%. Compared with DX56D, the UEL of AHSS samples are close to the TEL, i.e. the post uniform elongations are lower than DX56D. Meanwhile, 600 MPa AHSS have larger post uniform elongations than 800 MPa AHSS.

However, the strength of DX56D is the lowest which ultimate tensile strength (UTS) is 300 MPa. The UTS of other steels are in accordance with the steel grades where the UTS of 600 CP and DP steels are 668 MPa and 648 MPa, respectively, while UTS of 800 DP and CP steels are 865 MPa and 916 MPa, respectively.

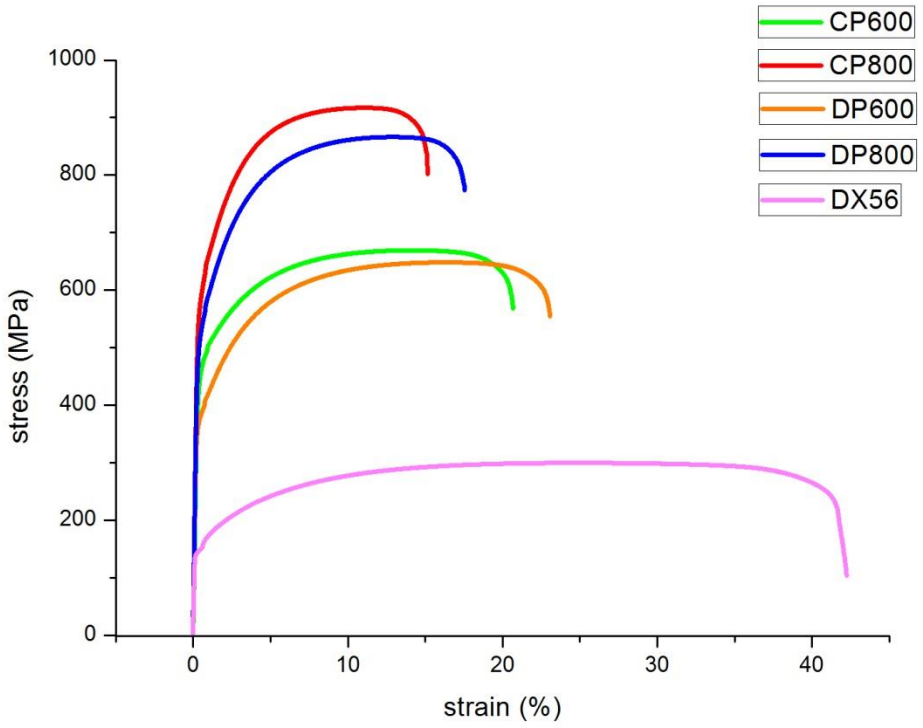

Figure 27.*Typical stress-strain curve of five sheet steels on rolling direction.*

6.1.2 Tensile Curve Interpretation

As estimation inputs, following 7 parameters are essential to acquire from tensile curves: yield strength (YS), ultimate tensile strength (UTS), yield ratio (YR), uniform elongation (UEL), UTS-UEL, total elongation (TEL), UTS-TEL.

OriginPro 8.0 which is a scientific graphic and data analysis software was used to analyze the stress-strain curve in this thesis. With the tensile data, OriginPro 8.0 can display the stress-strain curve and the data reader function of it provides an accurate and efficient way to acquire UTS, UEL and TEL directly from the curve. The value of Rp0.2 was determined as the yield strength, which is the strength value at the strain stage with 0.2% plastic deformation. To determine Rp0.2, the first step was to obtain the elastic deformation line by using linear fitting function of OriginPro 8.0. Next stage was to find the cross point of the elastic line and the tensile curve. Subsequently, the point on the tensile curve which strain was 0.2 higher than the previous cross point should be found. The strength value at this new point was then defined as Rp0.2. Values of UTS-UEL and UTS-TEL were calculated from UTS multiplies UEL and TEL, respectively. In addition, YR was calculated from YS divided by UTS. The required tensile data of five sheet steels on certain directions were listed in Appendix 1.

6.2 Experimental and estimation results comparison

As the main part of this thesis work, results of hole expansion tests and predicted HER values are introduced in this section. Brief comparisons between these two experiments are also included. Further discussions will be presented in next chapter.

6.2.1 Hole expansion test

Obviously, for 800 MPa grades steels, the hole diameters after tests are smaller than other sheet steels as Figure 28. (a) & (b) illustrate. In other words, the flangeabilities of CP800 and DP800 are worse than other strength grades steels.

An apparent result can be recognized that 600 MPa grade steels have better flangeabilities than 800 MPa steels since the final hole dimensions of 600 MPa steels are larger than 800 MPa steels in Figure 28. (c) & (d).

According to Figure 28. (e), the hole dimension of DX56D after the test is the largest among all the samples. This phenomenon illustrates that DX56D sample has much better flangeability than the previous four materials. As the figure shows, the final hole diameter is at least two times larger than 800 MPa steels.

In addition, the CP steels have better flangeability than DP steels under the same strength grade. In order to evidence this opinion, the exact data of the test results are listed in Table 2. In Table 2, the specimen column represents the material and number of each parallel specimen. While the punching position column represents the final position of the puncher. Both D avg and Dt avg are the average values of hole diameter which were calculated from two different direction measurements. Meanwhile, D indicates hole dimensions before the test while Dt represents the final hole dimensions after the test. HER column shows the hole expansion ratio of the test which was calculated from Equation 13. Moreover, the HER avg is the average value which was calculated from the HER value of those three parallel tests, the variance of each HER avg is listed in the bracket behind HER avg values.

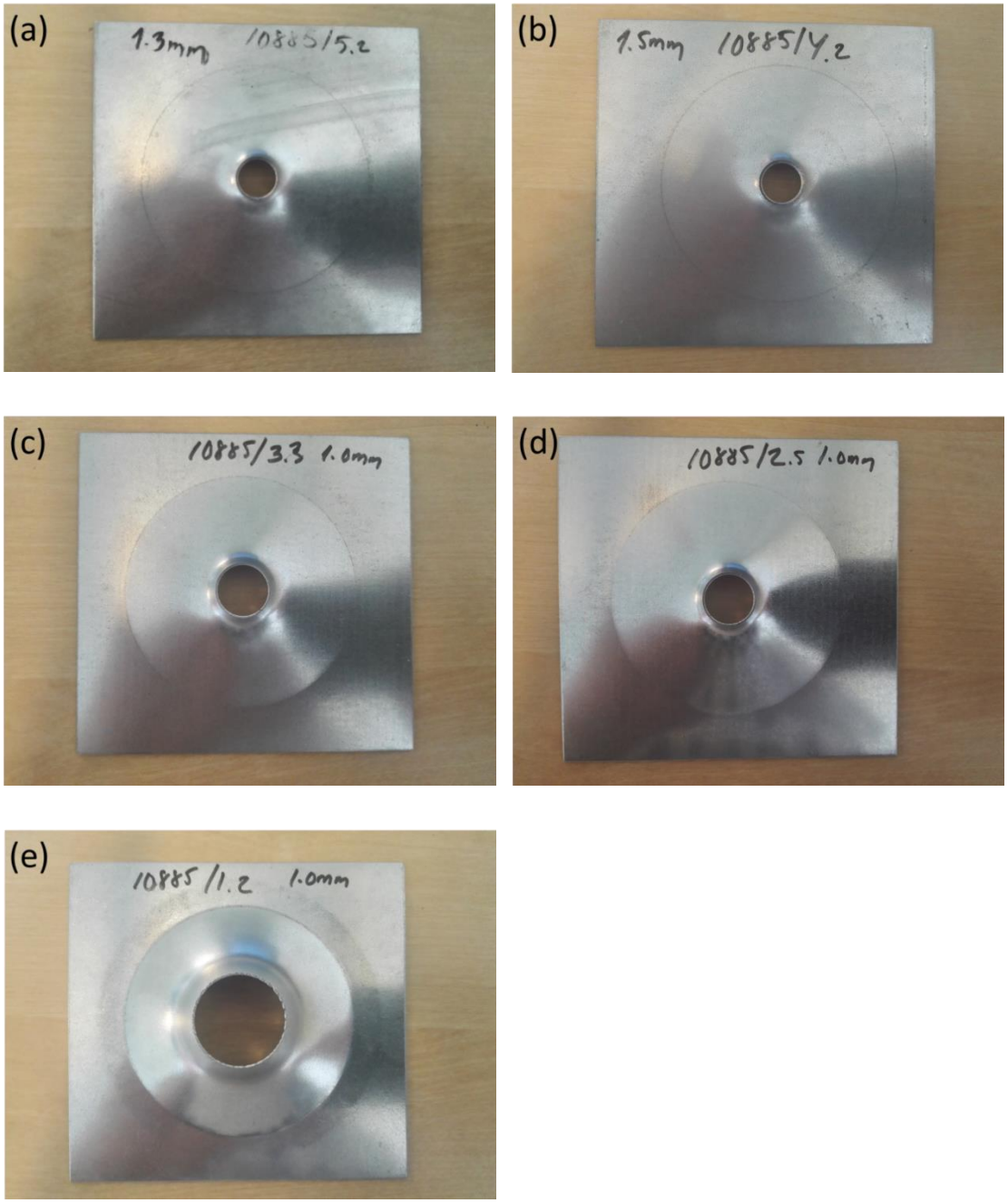

Figure 28.*Images of specimens after hole expansion tests. CP800 (a), DP800 (b), CP600 (c), DP600 (d), DX56D (e)*

As Table 2 illustrates, the flangeability of these sheet steels can be categorized into the following three groups. Apparently, the DX56D shows the best flangeability among all the samples, which HER reaches around 150%. Subsequently, the two 600 MPa grade steels 600 DP and 600 CP steels have lower flangeability, which HER values are about 40% and 50%, respectively. Furthermore, the lowest flangeability group includes 800 DP and 800 CP steels which HER values are around 17% and 19%, respectively.

Table 2.*Hole expansion test result*

Specimen	Punching position (mm)	D[a] avg. (mm)	Dt avg. (mm)	HER[b] (%)	HER avg. (%)
DX56D-1	37.9	10.0	25.2	151.1	151. 0 (±0.5)
DX56D-2	37.8	10.0	25.1	150.4	
DX56D-3	38.1	10.0	25.2	151.3	
DP600-1	19.9	10.0	14.6	45.0	40.2 (±4.2)
DP600-2	18.5	10.0	13.8	37.6	
DP600-3	18.5	10.0	13.9	37.9	
CP600-1	21.2	10.0	15.3	52.6	51.2 (±1.4)
CP600-2	20.6	10.0	15.0	49.8	
CP600-3	20.9	10.0	15.1	51.0	
DP800-1	16.0	10.1	11.8	17.0	17.0 (±0.8)
DP800-2	16.1	10.1	11.8	17.8	
DP800-3	15.7	10.1	11.7	16.1	
CP800-1	15.8	10.1	12.0	18.5	19.0 (±1.0)
CP800-2	15.8	10.0	11.9	18.4	
CP800-3	16.1	10.1	12.1	20.2	

a) D and Dt value were average value of measured diameters from two directions

b) Calculated by Equation 13

$$HER = (Dt - D) / D \times 100 \quad (13)$$

Based on testing results, it is apparent that the flangeability of the sheet steel was corresponding to the elongation property. In other words, sheet steel which had larger elongation showed better flangeability. This opinion can also explain the HER differences between DP and CP steels, which the CP steels showed better flangeability than DP steel under the same grades of strength.

6.2.2 HER estimation

HER estimation programs have already been introduced in Chapter 5, and the results of estimation are presented in this Section. The estimation results are classified into three groups according to the inputs of the results. Inputs of the results are derived by using tensile data on the transverse direction, rolling direction and 45^{o} from the rolling direction as program inputs, respectively. Furthermore, to be more convenient for the comparison, testing results are also listed in each table.

- Transverse direction

It can be seen from the Table 3, simulated results are various by using different models for the same materials and the feasibility of each model are different among the materials.

First, for the DX56D steel, the model 6 shows the best-simulated result (152.1%) which is almost the same as the testing result. Beside the model 6, the model 5 also shows a great feasibility for this steel, which the simulated result is 160.4%. While other models for DX56D show not that good feasibility as the model 5 and 6, the HER in model 1 is even twice larger than the testing result.

Table 3*.Estimation results by using transverse direction tensile data as the program inputs*

Steel grade	**Estimation HER value (%)**							
	Model 1	Model 2	Model 3	Model 4	Model 5	Model 6	Model 7	Test result
DX56D	386.8	115.0	194.1	170.0	160.4	152.1	108.3	151.0
DP600	80.3	61.0	91.5	68.1	68.4	63.6	106.4	40.2
CP600	52.4	53.6	45.5	50.1	50.6	45.2	98.9	51.2
DP800	26.7	28.6	36.8	25.9	30.7	32.4	107.1	17.0
CP800	42.0	28.0	36.2	25.7	30.5	32.4	108.3	19.0

Second, estimation programs show the highest feasibility for the CP600 steel among this group of prediction test. It can be seen from Table 3 that both model 1, 2, 4 and 5 present really close HER values as the testing result, which simulated results are 52.4%, 53.6%, 50.1% and 50.6%, respectively. Despite the model 3 and 6 show slightly infea-

sible for CP600 steel, the simulated HER still close to the testing result with 45.5% and 45.2%.

The situation of DP800 is similar to CP800 except the model 1 which CP800 shows a worse simulated result in this model. Despite the hole expansion test illustrated that CP800 have higher HER value than DP800 steel, but the simulated HER values in model 2 to 6 for these two steels are almost the same. For both of them, model 4 shows the best feasibility which HER of them in this model are 25.9% and 25.7%, respectively. However, these estimation values are still somewhat higher than the testing values which only have 17.0% and 19.0%.

Last, all these models in transverse direction group seem unsuitable for the DP600 steel, which results in all models have large differences compared with the testing result. Even in the relatively suitable model for DP600, the model 2 still has 61.0% HER value, which is somewhat higher than the testing HER (40.2%).

One phenomenon should be notice is that the steel type seems to have no effect on the result of model 7, which predicted results among all the materials remain slight fluctuation around 100%.

- Rolling direction

Table 4 presents the results of estimation programs by using tensile data on the rolling direction as the program inputs. Generally, the whole trend of the table is similar with Table 3 except some differences which can be categorized with the grades of strength.

First for the IF sheet steel DX56D, the most suitable model is still model 6 and other estimation models also present almost the same results as the transverse direction results. The largest difference between the results in Table 4 and Table 3 appeared in model 1 with 395.1% which is slight higher than the transverse direction result 386.8%, however both of them are too much higher than the testing result which only has 151.0% HER value.

Quite different with DX56D, the simulated HER of 600 MPa grade steels DP600 and CP600 have some extent changes compared with the transverse direction estimation. The most feasible models of 600 MPa grade steels are all changed. Model 6 predicts a result which more closed to the testing result for DP600 steel. Similar to the CP600 steel, the best model for CP600 has been changed from model 5 to model 1. Meanwhile, the most precise simulated results of 600 MPa grade steels have increase with different extent where the result of DP600 in model 6 slightly increases from 61.0% to 61.2%, while the simulated HER of CP600 increases from 50.6% to 53.3%. Another phenomenon of 600 MPa steels is that the simulated results from model 1 to 3 of DP600 steel are all promoted with several percentage points compared with the transverse direction results in these models, on the contrast, the later three models 4, 5 and 6 have lower HER

values compared with transverse direction results. However, for 600 CP steel, all the simulated results are promoted except the model 3 which shows a slight decline and promotion ranges of model 4, 5, 6 and 7 are much higher than the previous three models.

Table 4*.Estimation results by using rolling direction tensile data as the inputs*

Steel grade	**Estimation HER value (%)**							
	Model 1	Model 2	Model 3	Model 4	Model 5	Model 6	Model 7	Test result
DX56D	395.1	115.0	194.1	170.0	160.5	152.1	108.4	151.0
DP600	83.3	62.2	98.3	65.5	66.5	61.2	104.8	40.2
CP600	53.3	54.9	45.2	67.3	65.2	60.8	107.9	51.2
DP800	24.9	28.7	37.0	26.0	30.7	32.3	105.5	17.0
CP800	37.3	28.0	36.2	23.4	30.3	32.2	107.5	19.0

In 800 MPa grade steels, the model 1 becomes the most feasible model for DP800 while the model 4 is still the best model for 800CP. Compared with the transverse result, the outcomes of model 1 and model 4 in rolling direction drop and more close to the testing result, which model 1 shows 24.9% HER value for DP800 steel and model 4 shows 23.4% HER value for CP800 steel. For DP800, only model 1 and 6 generate lower HER value, while the other models generate higher values. For CP800 steel, model 1, 4, 5 and 6 generate lower HER values than transverse direction results, but model 2 and 3 present higher outcomes. Despite the general trend of each model has not changed, however, compared with the 600 MPa grade steels, the fluctuation range of 800 MPa steels are smaller than 600 MPa steels, which all the HER change within 3%. One exception is the result of model 1 for 800 CP, which decreases from 42.0% in the transverse direction to 37.3% in the rolling direction.

Moreover, model 7 outputs still remain stable around 100% which have not that much change among different materials. The results of each material in model 7 seem have slight fluctuation within 3% except CP600 which HER increases from 98.9% in the transverse direction to 107.9% in the rolling direction estimation result.

- 45^{o} from the rolling direction

Table 5 presents the estimation results of the selected models by using 45^{o} from rolling direction tensile data as the program inputs. In this group of estimation, results show various changing among different types of sheet steels.

As the above two directions results, the 45^{o} direction estimation results of DX56D remain stable, which the most feasible model for it is still model 6. Meanwhile, HER value in model 6 (152.1%) in 45^{o} direction only shows a slight increase than the model 6 results in transverse and rolling directions. Similarly, results of other models present almost the same HER values with the previous estimation results, the HER value fluctuation ranges are within 1%. However, model 1 still shows a worst stability when it compared with other models. The HER value in model 1 is 10% lower than the rolling direction result.

The result for DP600 steel on 45^{o} direction show massive differences by the comparison with the previous two direction results. HER values in all models except model 2 get larger than 10% differences than the results in transverse and rolling directions. Model 2 is again the most feasible model for DP600 on 45° direction with 63.7% HER. Moreover, model 2 is the relatively stable model for DP600, which HER differences between three direction estimation results are around 3%. Compared with transverse and rolling direction results, the HER values in model 1 and 3 are declined, in the contrast, outputs in other models are all improved with different extent.

For the CP600 steel, each model present different changes compared with the transverse and rolling direction results. In the 45^{o} estimation group, model 1 presents 52.9% simulated HER, which is most close to the testing result. Furthermore, model 1 is the most stable model for CP600. Similarly, the fluctuation of model 3 is also small, which result is slightly lower from around 45% in transverse and rolling directions to 42.9% on 45° direction. Compare with transverse and rolling direction results, the accuracy of model 2 is declined, which result on 45^{o} is 10% higher than the previous results. Results of the test model 4, 5, 6 and 7 all close with the results on the rolling direction with less than 3% differences. While both rolling and 45° direction results on these models have significant differences with the results on the transverse direction, the fluctuation ranges are 8%-18%.

Generally, the estimation results of DP800 in each direction are close. In the 45^{o} direction group, the best model for DP800 is the model 1 as well. Meanwhile, HER value in model 1 is 20.2% which is around 5% less than transverse and rolling results. Conversely, model 4 shows 31.2% HER, which is around 5% higher than transverse and rolling results of DP800. Compared with the previous results, HER values of the rest models are all slightly increased, however, the fluctuation ranges are less than 3%.

As the same grade steel, CP800 also has stable results and even better than DP800. The most feasible model among three directions tests is model 4 which simulated 25.1% HER in 45^o direction test. Meanwhile the value of model 4 HER result in 45^o direction is between the transverse and rolling direction results. Except the model 4, the results of model 1, 3, 5 and 6 are all between the previous two directions results range. Model 7 simulates a result which is steady increased while model 2 provides a steady decreased result. For CP800, fluctuation ranges of all models among 3 groups of tests are only around 1%. Model 1 as a special case for CP800 is also stable than the estimation results for other materials, which fluctuation range is around 5% among three groups of tests.

Table 5*.Estimation results by using 45 °from the rolling direction tensile data as the inputs*

Steel grade	**Estimation HER value (%)**							
	Model 1	Model 2	Model 3	Model 4	Model 5	Model 6	Model 7	Test result
DX56D	383.1	115.0	194.1	169.8	160.6	152.1	108.5	151.0
DP600	78.2	63.7	81.9	83.3	81.9	79.6	108.3	40.2
CP600	52.9	63.3	42.9	68.7	68.4	63.3	105.1	51.2
DP800	20.2	28.8	37.8	31.2	31.5	33.0	108.3	17.0
CP800	41.2	28.0	36.2	25.1	30.4	32.3	108.3	19.0

6.3 Feasibility of estimation programs

The accuracy of each estimation program is discussed in this section by comparing the error ratios which derived from the predicted results. Error ratios of all estimation models are calculated from the Equation 14 in order to compare the feasibility of each estimation program in a more convenient way. The error ratio can indicates the accuracy of the program, which the more the value close to zero, the higher accuracy the program is.

$$\text{Error ratio} = (\text{modeling result} - \text{testing result}) / \text{testing result} \times 100 \quad (14)$$

Appendix 2 presents the error ratio information of the whole estimation tests. The definition of ErN, Erm avg., $\bar{E}$rm avg. and Erp avg. are listed below Appendix 2. It is noteworthy that Erm avg. is calculated from the Equation 15.

$$\text{Erm avg.} = \frac{\sum_{N=1}^{7} |ErN|}{7} \quad (15)$$

Similarly, Erp avg. is calculated from the corresponding assumption of ErN absolute value divided by the amount of estimation tests which perform with the corresponding model.

To be more convenient for comparison, error ratio of each model on different selected materials and the error ratio comparison among three different direction inputs are presented as several bar charts in the following. In the bar charts, blue bars indicate the error ratio of the predicted results which were estimated by using transverse direction tensile data as the program inputs. Similarly, red bars denote the error ratio of the predicted results which were estimated by using rolling direction tensile data as the program inputs, while the green charts present the error ratio of the results on 45° from the rolling direction tensile data inputs. Meanwhile, $\bar{E}$rm avg. of each material is also presented in the bar charts as a dotted line.

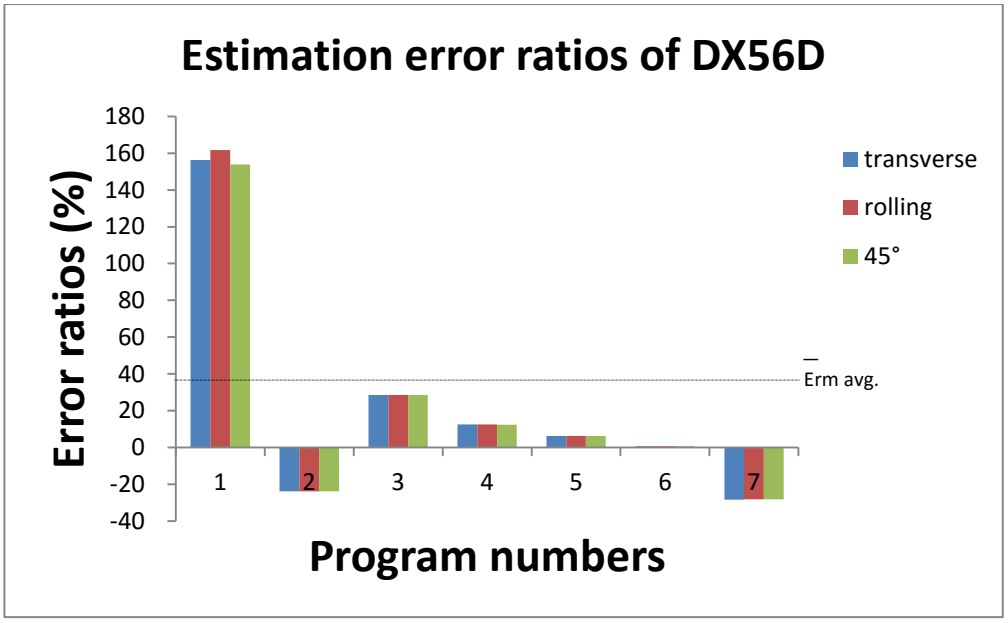

Figure 29.*Estimation error of DX56D sheet steel among 7 models with three direction tensile data inputs*

First comes to the DX56D sheet steel, one phenomenon can be found in Figure 29 is that the error ratios of all the models are steady which error ratios under different direction inputs are almost the same in model 2 to 7. Apparently, the most feasible model for DX56D is model 6 with the error ratio extremely close to zero which means there is almost no difference between simulated results and testing result. Meanwhile, error ratios of model 6 in three different directions have no fluctuation, which shows an excellent stability of this model. The error ratios of model 6 in transverse, rolling and 45° directions are 0.7%, 0.8% and 0.7%, respectively. For other models except model 1, the

values of the error ratios are from around 5% to 30%. The worst model for DX56D is model 1 which shows too much higher error ratios than other models, and the stability of model 1 is also worse than other models which error ratios among three direction inputs are 156.2%, 161.8% and 153.8%, respectively.

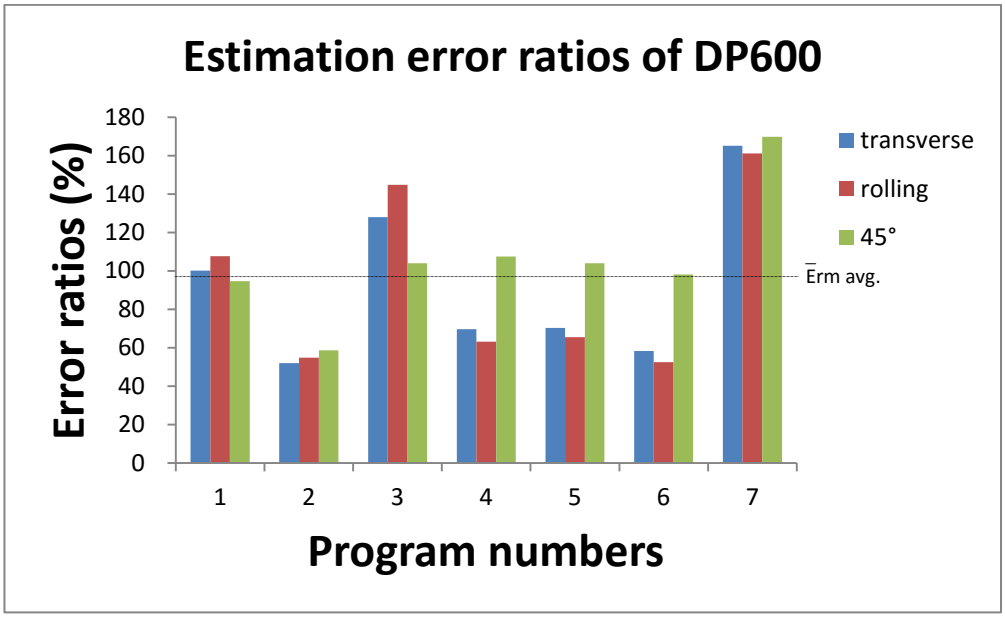

Figure 30.*Estimation error of DP600 sheet steel among 7 models with three direction tensile data inputs*

Compared with DX56D, error ratios for DP600 have massive diversity among different models with different inputs as Figure 30 shows. Generally, estimation error ratios of DP600 are much higher than DX56D, even model 2 which is the most feasible model for DP600 still has 52% error ratio by using transverse tensile data as the program inputs. On the inputs direction aspect, most models show a higher error ratio by using 45° tensile data as the program inputs. Even for model 1 and 3, the error ratio of 45° direction are still higher than the error ratios on other two directions in other models. In addition, transverse and rolling directions present close error ratios in most of the models and model 2 shows the lowest error ratio by using transverse tensile data as the program inputs.

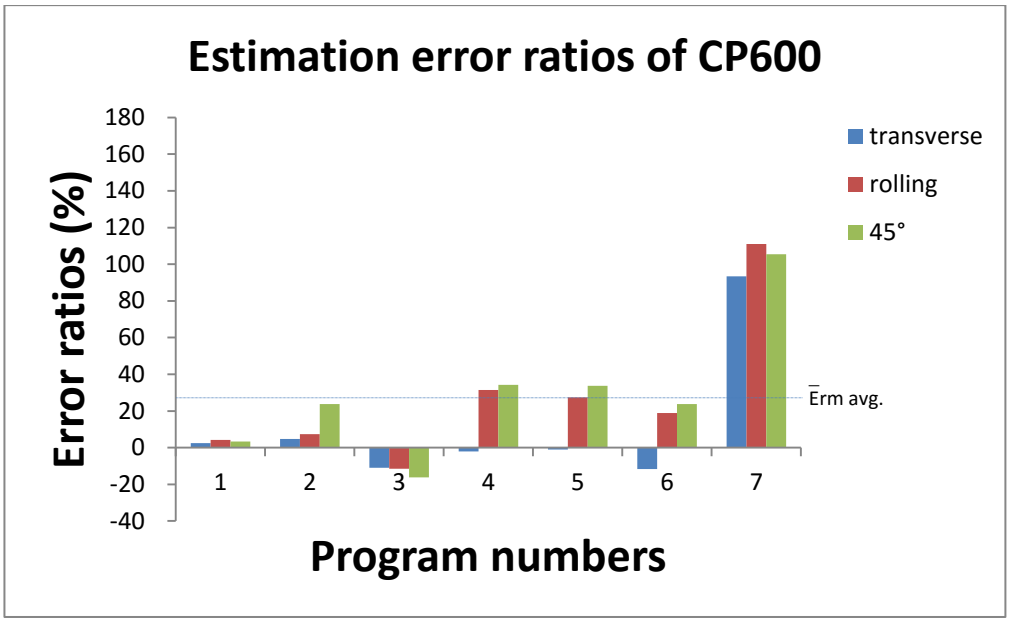

Figure 31.*Estimation error of CP600 sheet steel among 7 models with three direction tensile data inputs*

Negative error ratios appear in CP600 results as the columns of model 3 to 6 in Figure 31. The accuracy and trend of model 4 and 5 show an extreme similarity, which error ratios in the transverse direction are negative values and quite close to zero. Meanwhile, error ratios in other two directions are much higher than the transverse direction and the model 5 shows the best feasibility, which has only -1% error ratio in transverse direction estimation. Another phenomenon should be noticed is that the results in the transverse direction always present the lowest error ratio among three direction results in all these seven models. Furthermore, error ratios in model 1, 2 4 and 5 are all less than 5%, which show high accuracy of these models. Unlike the high accuracy of other models, all three direction inputs of model 7 have around 100% error ratios, which means the estimation HER values of model 7 are twice as much as the testing value.

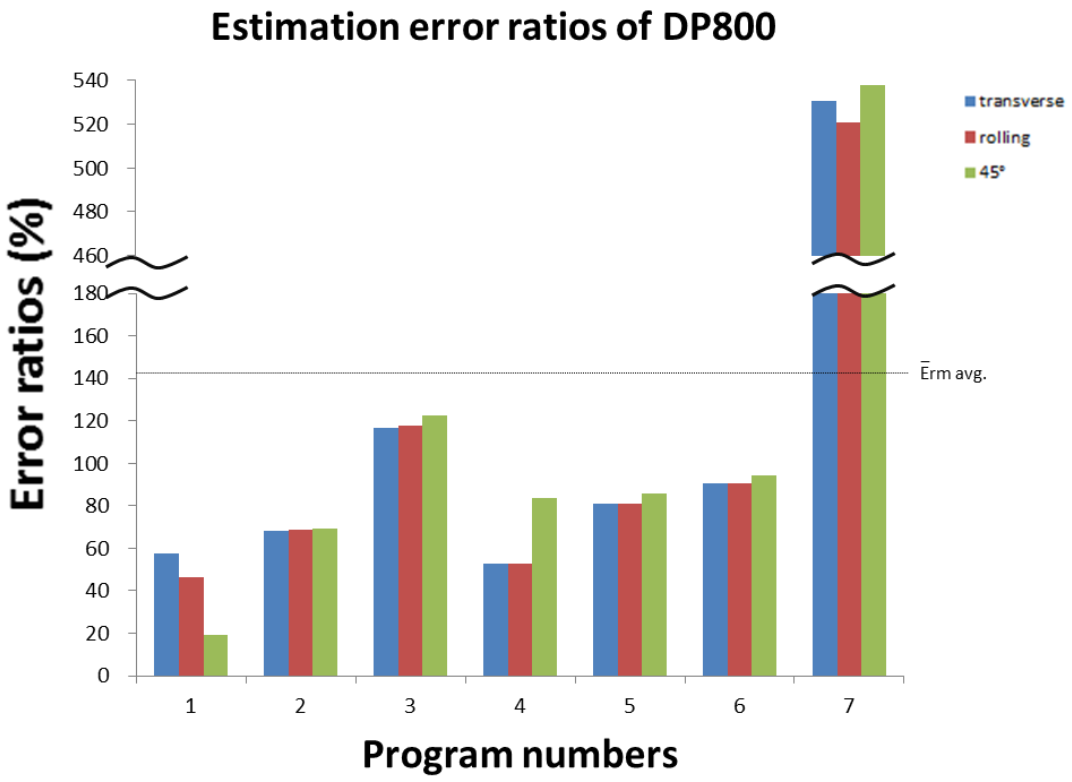

Figure 32.*Estimation error of DP800 sheet steel among 7 models with three direction tensile data inputs*

For the DP800 steel, most models generate similar error ratios among different direction estimations. As Figure 32 demonstrates, the best result of DP800 is acquired in model 1 by using tensile data on 45° direction as program inputs, which error ratio is 19.2%. Differently, the error ratios of model 1 are declined steadily from the transverse direction to 45° direction. In the contrast, the result of model 4 on 45° direction has a higher error ratio than the other two direction results. In addition, model 7 still has the highest error ratio among all the models with the average error ratio around 500%, which is even worse than the error ratios in 600 MPa grade steels.

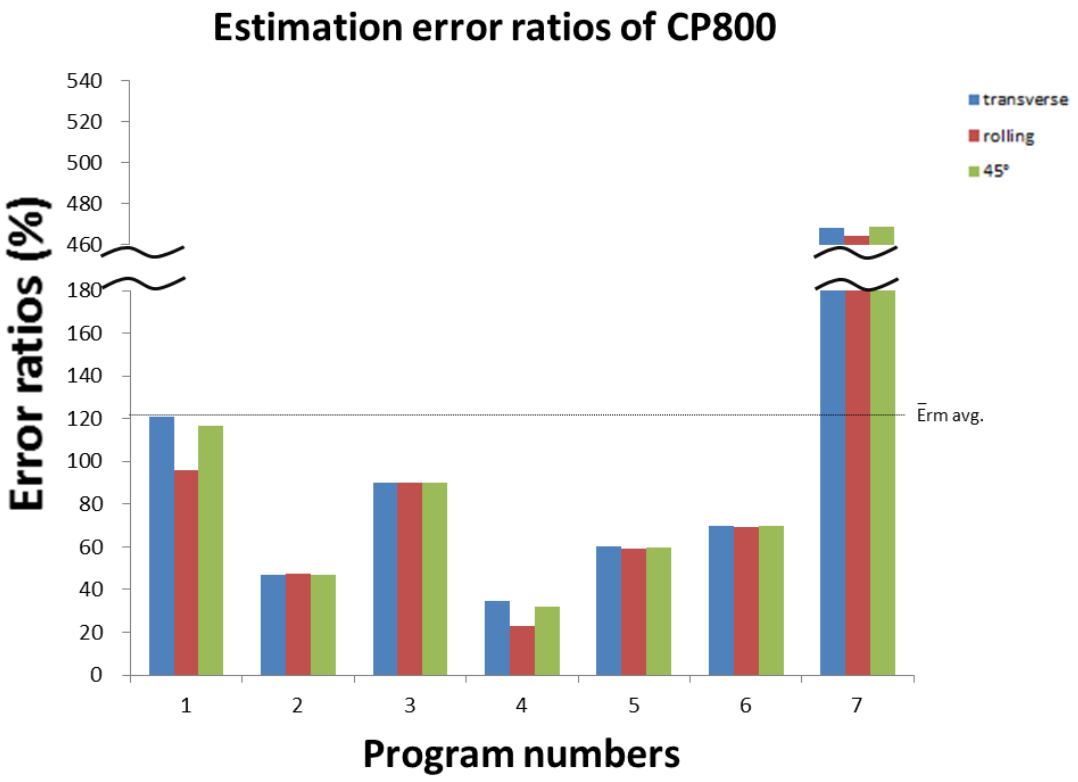

Figure 33.*Estimation error of CP800 sheet steel among 7 models with three direction tensile data inputs*

Similarly, CP800 steel also shows small fluctuation among different direction program inputs in all the models except model 1 and 4. In addition, the most feasible results in model 1 and 4 are both derived from the rolling direction inputs. Meanwhile, the best result presents in model 4, which error ratio is 23.1%. As Figure 33 illustrates, model 7 still shows too much higher error ratios than other models which error ratios on three directions are around 450%.

6.4 Fractures

In Section 6.4, the images of fracture observation under both optical and electron microscope of each sample are presented. Meanwhile, brief description of test results is also included. In addition, the scale bar of each image can be checked from the figure directly.

6.4.1 Optical microscope observation

Images of cross thickness fracture of each sample by using the optical electron microscope are presented as Figure 34. All these images were taken at the edge of punching holes where at least one cross thickness fracture can be clearly observed in the middle of the image.

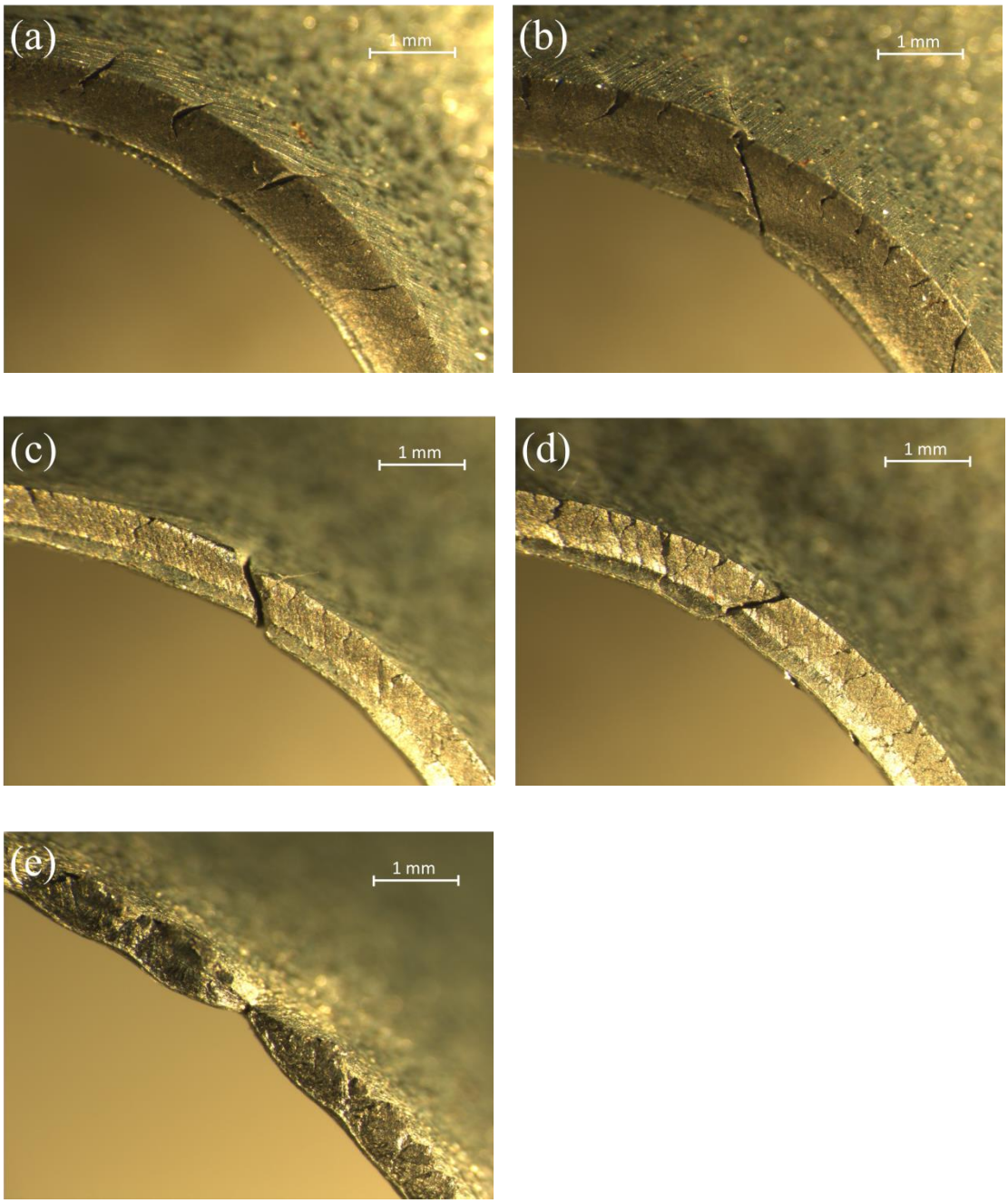

Figure 34.*Optical microscope images of cross thickness fractures. CP800 (a), DP800 (b), CP600 (c), DP600 (d), DX56D (e)*

In general, DX56D shows apparently different fracture edge than other selected materials. As can be seen from Figure 34, only DX56D has clear necking area around the cross thickness fracture which demonstrates a typical total ductile fracture. In the contrast, the fractures on other four samples show less ductile character than DX56D since the necking phenomenon are not apparent. Furthermore, deformations of hole edge on 600 MPa steels are serious than 800 MPa steels. Another phenomenon is that fewer cracks appear on CP steel samples when it compared with the same grade DP steel. One explanation is that 600 MPa steels have better ductility than 800 MPa steels and the

number of cracks is in negative correlation with the ductility of the steel. Considering the magnification limit of the optical microscope, more details of the fractures are presented in the electron microscope images from Section 6.4.2.

6.4.2 Electron microscope observation

The fracture observation results of the electron microscope are presented in this section. For all the presented figures in this section, the image (a) were taken under 50 ×magnifications, which showed the whole image around the cross thickness fracture, both cross section area and surface area can be observed in these images. Meanwhile, the rolling direction and transverse direction were noted as RD and TD at the right top corner of the figure. In addition, the image (b) were taken under 200× magnification which only showed the cross section area of the hole edge with more details of the cross thickness fracture.

As Figure 35. (a) shows, the cross thickness fracture propagates along a certain direction with a sharp edge on the surface. Unlike the surface condition, the crack shows a characteristic zigzag shape on the cross section area as Figure 35. (b) illustrates. In addition, some voids can be found on the cross section area of the punching hole, which are possible the initial voids of the crack. Moreover, small extent necking appears around the crack. As evidence, the right side of the crack is lower than the left side.

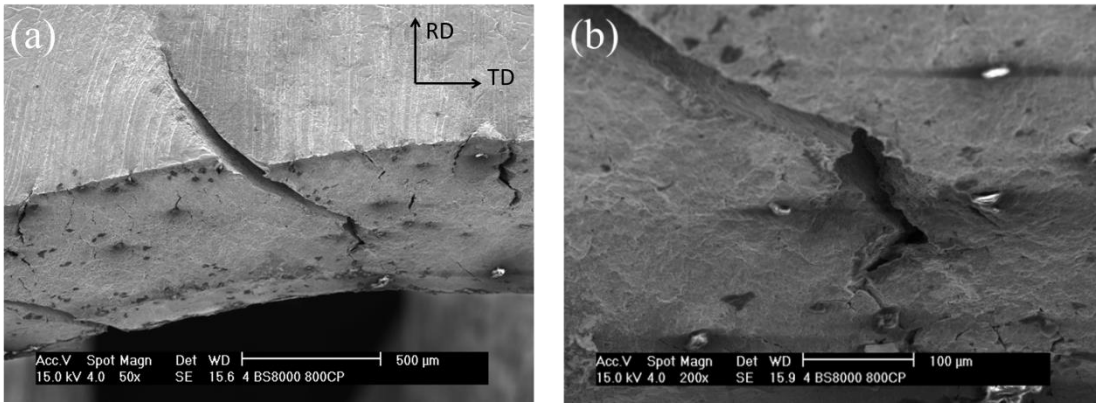

Figure 35.*SEM images of cross thickness fracture on CP800 hole expansion sample*

It is obvious that the ductility of DP800 steel is worse than other materials. As evidence, the crack on DP800 is totally straight forward. In addition, one phenomenon can be seen in Figure 36. (b) is that the cracking surface is quite smooth and some particles are split out from the crack. Generally, the crack of DP800 shows the trans-crystalline cleavage character.

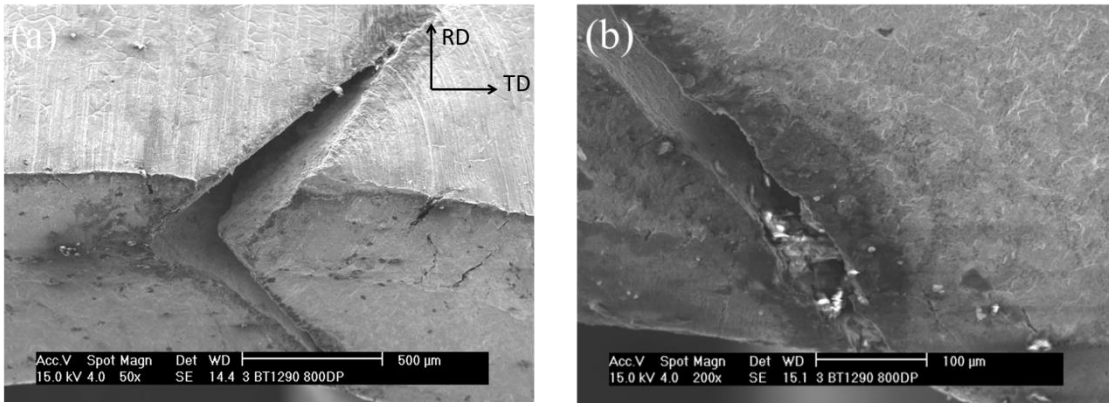

Figure 36.*SEM images of cross thickness fracture on DP800 hole expansion sample*

As the similar type steel with lower strength grade, CP600 shows more apparent necking around the cross thickness crack than CP800 steel. In Figure 37. (a), the crack is widely enlarged, and distinct deformation can be seen on the hole edge. Moreover, typical dimple textures can be found on the fracture region as Figure 37. (b) illustrates.

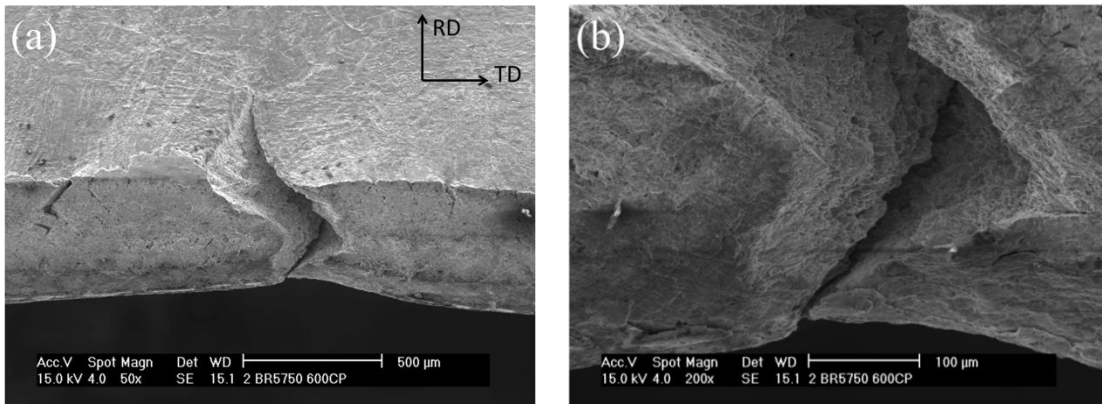

Figure 37.*SEM images of cross thickness fracture on CP600 hole expansion sample*

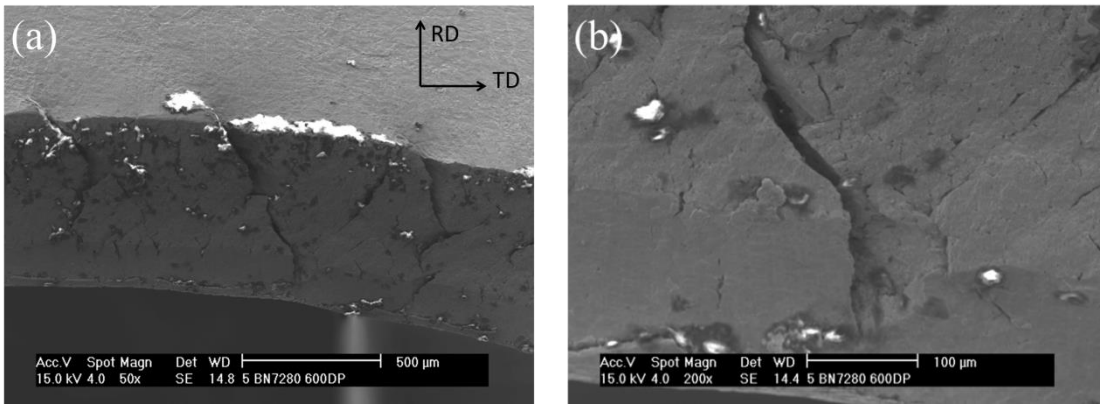

Figure 38.*SEM images of cross thickness fracture on DP600 hole expansion sample*

The condition for DP600 has some differences with the previous steels, which many small delamination cracks can be found at the cross section area as Figure 38. (b) shows.

Meanwhile, the directions of delamination cracks are uncertain. In addition, some cross section surfaces are split down by the effect of delamination cracks.

For the formable material DX56D, the SEM images show much better ductility of it than other samples, which a large necking area can be found clearly according to Figure 39. However, the edge of the punching hole is hard to distinguish because the edge is also deformed due to the high formability. With higher magnification lamellar structures can be found on the cross section area. One thing should be noticed is that the direction and density of lamellar structures can be affected by the stress direction. In other words, lamellar structures can indicate the stress direction.

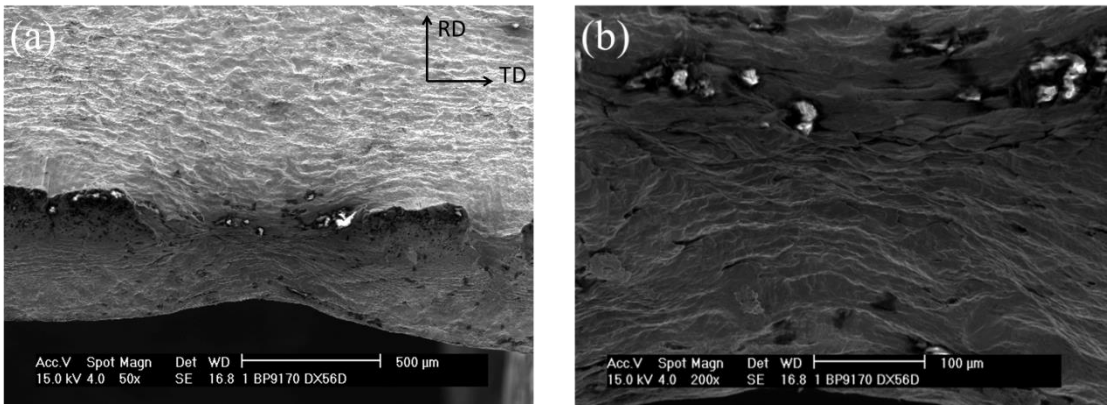

Figure 39.*SEM images of cross thickness fracture on DX56D hole expansion sample*

7. DISCUSSION

Apparently, some programs for certain material presented extremely accurate simulated results while others showed inaccurate results. In Chapter 7, the feasibility of each estimation programs and possible reasons for inaccuracy are discussed.

Considering the estimation test is a kind of black box testing, which the specific program codes are sealed. Therefore, the feasibility of models cannot be discussed on the interior factors of model programming. Alternatively, feasibility differences are mainly discussed on materials aspect in this thesis. On one hand, the feasibilities differences are analyzed by comparing the microstructures among each material. On the other hand, the feasibility of models are also correlate with the fracture differences since each sheet steels presented different edge fractures during the hole expansion test.

Another explanation for the inaccuracy of the estimation HER should be the modelling programs. Despite the interior source code of estimation programs are sealed, however, the inputs requirements of each program are diverse and already known. Therefore, inputs parameter selection can be a factor which affects the final estimation results since different indexes and directions of the tensile data provided diverse simulated results. In addition, as the algorithm system, ANN has some defects which can be an influential factor for the final estimation results.

7.1 Material analysis

7.1.1 Microstructures

With the $\overline{E}$rm avg. in Appendix 2, the overall feasibility of all programs on selected steel sheet can be revealed. Generally, the estimation feasibilities of these programs have positive correlation with the test HER of the applied material. In other words, estimation error ratios decrease with the test HER value of the applied material increases. An exception is the $\overline{E}$rm avg. of DX56D which is higher than $\overline{E}$rm avg. of CP600 steel. For DX56D, all the programs simulate relative steady and accurate results except model 1. However, the average error ratio of DX56D can be dramatically reduced if the results from model 1 not take into account.

Moreover, estimation models provide more precise results for lower strength grade steels, since the $\overline{E}$rm avg. of 600 MPa grades steels are smaller than 800 MPa grades steels. Meanwhile, tested HER of AHSS are also in accordance with the above point of view. On the steel type aspect, estimation programs are more feasible for CP steels than

the same grade DP steels. This result may refer to the phase difference which is more complicated in CP steels than DP steels. Meanwhile, phases hardness difference in CP steel is larger than DP steel, which work hardening of ferrite reduce the hardness difference between martensite and ferrite. According to $\bar{E}$rm avg., there is a tendency that selected programs are more feasible for large phase difference as well as large hardness difference sheet steels. Some more regular patterns can be concluded through microstructure comparison between different materials as following.

According to Figures in 5.1.2, a conspicuous difference is the amount of hard phases. With the proportion of hard phases increase, the $\bar{E}$rm avg. of steels is decreasing. For the IF steel DX56D, common hard phases are carbides and nitrides, which used to stabilize the steel (i.e. to bind free carbon and N into nitrides and carbides). Both these hard phases disperse in large grain ferrite with a preferential texture {111} which provides an extremely good formability for the steel. While in AHSS, common hard phases are martensite in DP steels and bainite in CP steels, which disperses within the ferrite matrix as the secondary hardening phases. It is known that bainite and carbide have lower hardness than martensite which increases the strength of sheet steels. Meanwhile, the test HER values are increased with the strength of steels promoted, which is also in accordance with the phenomenon that $\bar{E}$rm avg. increases with the test HER of the sheet steels increase.

Another difference is the shape of hard phases. On the same strength grade, the edges of hard phases in CP steels are smoother than those hard phases in DP steels. Thus, an explanation is that the grain refinement can affect the HER estimation results which estimation programs are more feasible for the sheet steels with fine shape hard phases microstructure.

The third factor is the uniform of hard phases. The effect of the uniform is not that much influence on the final estimation results when it compared with the other influence factors. On 800MPa grade, the size differences between different hard phases in CP steel are smaller than the differences in DP steel. Meanwhile, the cementite in DX56D has the smallest size when it compared with martensite and carbide in AHSS. Therefore, the particle differences of DX56D are the smallest in all the five materials. By take the $\bar{E}$rm avg. into account, a phenomenon can be concluded, which estimation programs are more feasible for the sheet steels with higher uniform hard phases. However, the strength of the steel should first take into account. For the circumstances which the results between strength and uniform are inconsistent, the error ratios are changed according to the correlation with strength and the effect of uniform should be ignored under this circumstance.

The last factor which affects the feasibility of estimation programs is the alignment condition of hard phases i.e. the microstructural banding condition. Referring to the microstructure images, 800 MPa grades steels have distinct microstructural banding

phenomena compare with 600 MPa steels. Despite the DX56D also shows a distinct microstructural banding, the amount of banding phases are less than 800 MPa steels. Therefore, the selected estimation programs are more feasible for the steels which have less microstructural banding characters.

7.1.2 Fracture differences

Section 7.1.1 provided a tendency which $\bar{E}$rm avg. increases with the testing HER of sheet steel improves. However, as the same strength grade steels, the $\bar{E}$rm avg. of DP600 was much larger than $\bar{E}$rm avg. of CP600. In this thesis, fracture comparison is essential.

According to Figure 37 and 38, the biggest difference between CP600 and DP600 is the formation of the cross thickness fracture. In CP600 steel, the cross thickness fracture is generated by voids nucleation, growth and coalescence with large deformation at the hole edge. While for DP600 steel, the deformation condition at hole edge is worse than CP600 steel and the cross thickness fracture on DP600 is generated from delamination cracks which are not appeared in other sheet steels either.

Furthermore, the hole edge necking phenomenon of DX56D and CP600 are much apparent than other materials, which are in accordance with the $\bar{E}$rm avg**.** of these two materials. As a consequence, necking is an important factor which has the positive effect on program estimations.

7.2 Program analysis

7.2.1 Inputs selection

As the basic variable between those models, the inputs of programs should take into account. By analyze the most feasible program for each material, some rules for the inputs selection can be summarized.

With the Erp avg. in Appendix 2, the generic feasibility of each estimation program can be seen. In general, if a program is suitable for most materials, the accuracy of it is medium. For example, in most cases, program 2 and 4 present the medium error ratios when compared with other programs for the same material. However, accuracies in these cases are not high enough. Even for DP600 and CP800 steels which program 2 and 4 are the most feasible programs for them, the estimation error ratios are still have 52% and 23% respectively.

In the contrast, if a program has high accuracy for specific steel, the estimation program can only suit several certain materials while have large fluctuation among other type

steels. An instance is the program 6 which only has 0.7% error ratio for DX56D HER prediction while for DP600 steel, the error ratio on 45^{o} direction can reach 98.2%.

Another tendency is that for most materials, the estimation accuracy improved with the number of input parameter increased. Such as for DP800 and CP800 steels, the best programs are program 1 and 4, respectively, both programs need 5 different input parameters. While for the program 7 which only has one required input, the estimation results is turned to be the worst among all the programs and materials. In fact, a similar result was discovered by Raj et. al. before, since the prediction of the formability on stainless steel sheet performed better accuracy with large amount of parameters be used as program inputs. [72]

On the aspect of specific parameter selection, the UTS seems to be the most essential parameter for the HER estimation. The evidence is that error ratios of program 3 and 7 are much higher than those programs which use UTS as one of the program inputs.

On the other hand, parameter selection has the correlation with steel types. Based on error ratios from Appendix 2, the best programs for DP steels are program 2 and 1 which use UEL as one of the program inputs. While for CP steels, the best programs are 5 and 4, which have almost the same inputs with DP steels. The only difference is that UEL is replaced by TEL. In addition, for DX56D, the inputs in program 6 have neither UEL nor TEL but use UTS-TEL as an input which has the elongation information.

Despite sheet steels have anisotropy characters, the simulated HER values are close by using different direction tensile data as program inputs. But a tendency can still be summarized according to Erm avg. of those programs. Generally, DX56D with 45^{o} direction tensile data performs the best estimation results. Meanwhile, 600 MPa grade steels prefer the transverse tensile data to get a better estimation results. Furthermore, rolling direction tensile data leads to lower Erm avg. than other two directions for 800 MPa grade steels.

7.2.2 Disadvantage of artificial neural network

In addition, as a program training method, ANN has some intrinsic disadvantage which cannot avoid and might be a reason to cause the inaccurate on the estimation results. The first and most frequent drawback of ANN is the overfitting during program training. As introduced in Section 4.1 that ANN uses linear regression to find the correlation between inputs and target parameter. However, the linear equation might extremely suitable for a certain training data but the accuracy for general cases is low. To reduce the overfitting effect on ANN program, experiment data can be divided into two groups, one group is used as training data, and another group is used to check the accuracy of the model. [59]

Another defect of ANN is the datasets volume requirement. Since the fundamental of ANN training process is to train programs by using experiment data, then, deduce a suitable correlation equation. A large capacity dataset is essential to deduce a precise model, thus with the data increase, the accuracy of the model can be increased and avoid overfitting circumstance which caused by lack of training data. One solution for this is to use more experimental data in the training process of program which can add various experiment data into correlation deduction. This can also be used to explain the result which more number of parameters can increase the generality of the estimation program. [73]

8. CONCLUSION

In this master thesis, seven HER estimation programs were used to compare the estimation HER values with the hole expansion test results on five different sheet steels. Moreover, microstructures and hole edge fractures of these samples were observed by both optical and scanning electric microscopes in order to analyze the differences between testing and estimated HER results.

According to the estimation results, the most feasible programs for each sheet steels are as following:

For DX56D, the most feasible estimation program is program 6. The error ratio of the most accurate estimation result is 0.7% by using 45° direction tensile data as the program inputs.
For DP600, the most feasible estimation program is program 2. The error ratio of the most accurate estimation result is 52.0% by using transverse direction tensile data as the program inputs.
For CP600, the most feasible estimation program is program 5. The error ratio of the most accurate estimation result is -1.0% by using transverse direction tensile data as the program inputs.
For DP800, the most feasible estimation program is program 1. The error ratio of the most accurate estimation result is 19.2% by using 45° direction tensile data as the program inputs.
For CP800, the most feasible estimation program is program 4. The error ratio of the most accurate estimation result is 23.1% by using rolling direction tensile data as the program inputs.

The comparison results demonstrate that none of these prediction programs are feasible for sheet steels of every kind. The estimation results have huge fluctuation among different materials within each program, which the error ratios are diverse from 0.7% to 537.7%. Meanwhile, the program 7 is the worst program in all the selected programs, which Erp avg. of it is 258.7%.

Nevertheless, several tendencies can be concluded according to estimation error ratios. First, with the strength grade increased, the error ratios of prediction programs are increased. Meanwhile, CP steels show better estimation accuracy than the same strength grade DP steels. Furthermore, SEM images illustrate that microstructure differences are the possible reason for prediction fluctuations where grain refinement and uniform of hard phases have positive influence on the predicted results. Conversely, the amount of

hard phases has negative influence. Moreover, the selected estimation programs are more feasible for the sheet steels with diverse phase microstructures and large hardness difference between different phases. Furthermore, these programs show better feasibility for the sheet steels which have less microstructural banding phenomenon.

Second, the steel which the cross thickness fracture generated from voids formation shows the better simulated result than the same grade steel which contains delamination cracks at the hole edge of hole expansion samples. On the other hand, the steels which show necking phenomenon at the hole edge of hole expansion samples perform better simulated results.

On the aspect of input selection, the Erm avg. shows a tendency which 45° , transverse and rolling direction tensile data perform the best predicted results for DX56D, 600 MPa and 800 MPa grades steels, respectively. While the anisotropy of sheet steel only has small effect on the estimation accuracy since three direction inputs lead steady prediction results for most materials. Moreover, in the input parameter selection, the most significant parameter is the UTS which directly indicates the strength level of sheet steel.

Last trend is that a program which can predict the HER value with a high accuracy for a certain material always shows low generality for other materials, vise versa. In general, the accuracies of estimation programs are increased with the number of program inputs increase. On the other hand, absence of training dataset and overfitting in the linear regression process of ANN training can be the main reason for this phenomenon.

In conclusion, these prediction programs still cannot replace the laboratory hole expansion test for all kinds of sheet steels due to lack of accuracy for some certain type materials. However, for formable sheet steels, some programs show high accuracy, which can be used to predict or calibrate the testing results. Therefore, for specific sheet steel, the selection for a suitable estimation program is important. Moreover, to get more precise prediction results, new training methods or programming methods are essential to improve the feasibility of estimation programs.

APPENDIX 1: TENSILE DATA

Steel grade	Directions	YS [MPa]	UTS [MPa]	TEL %	YR	UTS-TEL [MPa-%]	UEL %	UTS-UEL
DX56D	rolling	144	300	42	0.480	12600	25	7500
	transverse	150	299	43	0.502	12857	24	7176
	45 degree	153	305	41	0.502	12505	24	7320
DP600	transverse	372	651	22	0.571	14322	16	10416
	rolling	366	648	23	0.565	14904	16	10368
	45 degree	384	644	20	0.596	12880	19	12236
CP600	transverse	440	672	24	0.655	16128	14	9408
	rolling	441	668	20	0.660	13360	14	9352
	45 degree	454	645	23	0.704	14835	17	10965
DP800	transverse	525	872	16	0.602	13952	13	11336
	rolling	516	865	17	0.597	14705	13	11245
	45 degree	495	861	12	0.575	10332	11	9471
CP800	transverse	602	920	11	0.654	10120	10	9200
	rolling	582	916	15	0.635	13740	11	10076
	45 degree	602	926	11	0.650	10186	11	10186

APPENDIX 2: ERROR RATIOS OF ESTIMATION PROGRAMS

Steel grade	Input directions	Error ratios of estimation programs (%)								
		Er1[a)]	**Er2**	**Er3**	**Er4**	**Er5**	**Er6**	**Er7**	**Erm[b)] avg.**	**$\bar{E}$rm[c)] avg.**
DX56D	transverse	156.2	-23.8	28.6	12.7	6.3	0.7	-28.2	36.6	36.8
	rolling	161.8	-23.8	28.6	12.6	6.4	0.8	-28.2	37.4	
	45 °	153.8	-23.8	28.6	12.5	6.4	0.7	-28.1	36.3	
DP600	transverse	100.1	52.0	127.9	69.6	70.4	58.3	165.1	91.9	96.6
	rolling	107.6	54.8	144.8	63.1	65.6	52.4	161.1	92.8	
	45°	94.7	58.6	104.0	107.4	104.0	98.2	169.7	105.2	
CP600	transverse	2.4	4.7	-11.0	-2.0	-1.0	-11.6	93.4	18.0	27.5
	rolling	4.2	7.4	-11.5	31.5	27.5	18.9	111.0	30.3	
	45°	3.4	23.8	-16.1	34.2	33.7	23.8	105.4	34.3	
DP800	transverse	57.3	68.1	116.7	52.5	80.8	90.5	530.7	142.4	142.2
	rolling	46.3	68.9	118.0	52.8	80.9	90.4	520.8	139.7	
	45°	19.2	69.4	122.4	83.4	85.5	94.2	537.7	144.6	
CP800	transverse	120.8	47.1	89.9	34.7	60.1	69.9	468.6	127.3	124.9
	rolling	96.1	47.2	90.1	23.1	59.3	69.2	464.4	121.4	
	45°	116.5	46.8	89.9	31.8	59.9	69.7	468.7	126.2	
Erp[d)] avg.		82.7	41.3	75.2	41.6	49.8	50.0	258.7		

a) ErN denotes the error ratios in program N

b) Erm avg. denotes the average error ratios for a certain material among 7 estimation programs on each direction

c) $\bar{E}$rm avg. denotes the total average error ratios for a certain material among 7 estimation programs on three directions

d) Erp avg. denotes the average error ratios for a certain estimation programs among 5 materials on all inputs directions

REFERENCES

[1] Barthel C, Klusemann B, Denzer R, et al. Modeling of a thermomechanical process chain for sheet steels[J]. International Journal of Mechanical Sciences, 2013, 74: 46-54.

[2] Panich S, Barlat F, Uthaisangsuk V, et al. Experimental and theoretical formability analysis using strain and stress based forming limit diagram for advanced high strength steels[J]. Materials & Design, 2013, 51: 756-766.

[3] MAP: Background information. [WWW] http://www.msm.cam.ac.uk/map/backg.html#aim

[4] CustoMPart.net: Sheet metal fabrication. [WWW] http://www.custoMPartnet.com/wu/sheet-metal

[5] SSAB: History of sheet steel. [WWW] http://www.ssab.com/en/Brands/Greencoat/Products/What-is-Prelaq/Brief-history-of-sheet-steel/

[6] Metal working world magazine: A short sheet metal history. [WWW] http://www.metalworkingworldmagazine.com/a-short-sheet-metal-history/

[7] Kuziak, R., R. Kawalla, and S. Waengler. "Advanced high strength steels for automotive industry." Archives of civil and mechanical engineering 8.2 (2008): 103-117.

[8] Rukki Metals: Litec advanced high-strength steel brochure. [WWW] http://www.ruukki.com/Steel/Metal-coated-steels/Litec-advanced-high-strength-steel

[9] Rocha R O, Melo T M F, Pereloma E V, et al. Microstructural evolution at the initial stages of continuous annealing of cold rolled dual-phase steel[J]. Materials Science and Engineering: A, 2005, 391(1): 296-304.

[10] Kuziak, R., R. Kawalla, and S. Waengler. "Advanced high strength steels for automotive industry." Archives of civil and mechanical engineering 8.2 (2008): 103-117.

[11] Chakraborti P C, Mitra M K. Microstructure and tensile properties of high strength duplex ferrite–martensite (DFM) steels[J]. Materials Science and Engineering: A, 2007, 466(1): 123-133.

[12] WorldAutoSteel: Automotive Steel Definitions. [WWW] http://www.worldautosteel.org/steel-basics/automotive-steel-definitions/

[13] Zhao H, Rama S C, Barber G C, et al. Experimental study of deep drawability of hot rolled IF steel[J]. Journal of Materials Processing Technology, 2002, 128(1): 73-79.

[14] Thomas H. Courtney. Mechanical Behavior of Materials. Waveland Press, 2. Edition, 2005.

[15] Barnett M R, Kestens L. Formation of {111}< 110> and {111}< 112> Textures in Cold Rolled and Annealed IF Sheet Steel[J]. ISIJ international, 1999, 39(9): 923-929.

[16] Raabe D, Hantcherli L. 2D cellular automaton estimation of the recrystallization texture of an IF sheet steel under consideration of Zener pinning[J]. Computational Materials Science, 2005, 34(4): 299-313.

[17]Galfan technology centre: About Galfan. [WWW] http://galfan.com/

[18] Jiang H M, Chen X P, Wu H, et al. Forming characteristics and mechanical parameter sensitivity study on pre-phosphated electro-galvanized sheet steel[J]. Journal of Materials Processing Technology, 2004, 151(1): 248-254.

[19] Bressan J D, Hesse R, Silva E M. Abrasive wear behavior of high speed steel and hard metal coated with TiAlN and TiCN[J]. Wear, 2001, 250(1): 561-568.

[20] Schuerz S, Fleischanderl M, Luckeneder G H, et al. Corrosion behaviour of Zn–Al–Mg coated steel sheet in sodium chloride-containing environment[J]. Corrosion Science, 2009, 51(10): 2355-2363.

[21] Arcelor: Metallic coated steel user manual. Available at: http://www.szs.ch/user_content/editor/files/Downloads_Stahlwerkstoffe/metallic%20coated%20steel.pdf

[22] Wang W, Wei X. The effect of martensite volume and distribution on shear fracture propagation of 600–1000MPa dual phase sheet steels in the process of deep drawing[J]. International Journal of Mechanical Sciences, 2013, 67: 100-107.

[23] Wang X, Li L, Deng L, et al. Effect of forming parameters on sheet metal stability during a rotary forming process for rim thickening[J]. Journal of Materials Processing Technology, 2015, 223: 262-273.

[24] Zhao Z Z, Yin H X, Zhao A M, et al. The influence of the austempering temperature on the transformation behavior and properties of ultra-high-strength TRIP-aided bainitic–ferritic sheet steel[J]. Materials Science and Engineering: A, 2014, 613: 8-16.

[25] Shiozaki T, Tamai Y, Urabe T. Effect of Residual Stresses on Fatigue Strength of High Strength Steel Sheets with Punched Holes[J]. International Journal of Fatigue, 2015.

[26] AZO Materials: the future of steel in the automotive industry. [WWW] http://www.azom.com/article.aspx?ArticleID=10538

[27] CSSBI: Who choose sheet steel [WWW] http://cssbi.ca/

[28] Steel designers' manual[M]. John Wiley & Sons, 1972, 40(35): 887-902.

[29] KSS shutters: sheet metal roofing. [WWW] http://www.kssthailand.com/products/sheet-metal-roofing/

[30] CSSBI: CN-SBS PROJECT [WWW] http://cn-sbs.cssbi.ca/

[31] Loveday M S, Gray T, Aegerter J. Tensile testing of metallic materials: a review[J]. Final report of the TENSTAND project of work package, 2004, 1.

[32] Instron: Tensile testing. [WWW] http://www.instron.com/sv-se/our-company/library/test-types/tensile-test?region=Sweden

[33] SlideShare: Behaviour of Materials. [WWW] http://www.slideshare.net/engCETL/tta104-section-4

[34] NDT Resource center: Tensile properties. [WWW] https://www.nde-ed.org/EducationResources/CommunityCollege/Materials/Mechanical/Tensile.htm

[35] Funakawa Y, Inazumi T, Hosoya Y. Effect of morphological change of carbide on elongation of boron-bearing Al-killed steel sheets[J]. ISIJ international, 2001, 41(8): 900-907.

[36] Li D, Ghosh A. Tensile deformation behavior of aluminum alloys at warm forming temperatures[J]. Materials Science and Engineering: A, 2003, 352(1): 279-286.

[37] Chiriac C, Chen G. Local Formability Characterization of AHSS–Digital Camera Based Hole Expansion Test Development[C]//Best in Class Stamping, Proceedings of the International Deep Drawing Research Group (IDDRG) 2008 Conference. Swedish Deep Drawing Research Group, Olofström, Sweden, 2008: 81-91.

[38] Stachowicz F. Estimation of hole-flange ability for deep drawing steel sheets[J]. Archives of Civil and Mechanical Engineering, 2008, 8(2): 167-172.

[39] Ko Y.K., Lee J.S., Huh H., Kim H.K., Park S.H.: Prediction of fracture in hub-hole expanding process using a new ductile fracture criterion, J. Mat. Proc. Technol., Vol. 187–188, 2007, pp. 358 – 362.

[40] Mori K, Abe Y, Suzui Y. Improvement of stretch flangeability of ultra high strength steel sheet by smoothing of sheared edge[J]. Journal of Materials Processing Technology, 2010, 210(4): 653-659.

[41] Obermeyer E J, Majlessi S A. A review of recent advances in the application of blank-holder force towards improving the forming limits of sheet metal parts[J]. Journal of Materials Processing Technology, 1998, 75(1): 222-234.

[42] Sugimoto K, Sakaguchi J, Iida T, et al. Stretch-flangeability of a high-strength TRIP type bainitic sheet steel[J]. ISIJ international, 2000, 40(9): 920-926.

[43] Keeler S, Kimchi M. Advanced High-Strength Steels Application Guidelines V5[M]. WorldAutoSteel, 2015: 68.

[44] Hasegawa K, Kawamura K, Urabe T, et al. Effects of microstructure on stretch-flange-formability of 980 MPa grade cold-rolled ultra high strength steel sheets[J]. ISIJ international, 2004, 44(3): 603-609.

[45] Paul S K, Mukherjee M, Kundu S, et al. Prediction of hole expansion ratio for automotive grade steels[J]. Computational Materials Science, 2014, 89: 189-197.

[46] Baosteel: Testing items. [WWW] http://esales.baosteel.com/baosteel_products/commercialVehicle/en/material/material_03_01.jsp

[47] Westermann I, Snilsberg K E, Sharifi Z, et al. Three-point bending of heat-treatable aluminum alloys: influence of microstructure and texture on bendability and fracture behavior[J]. Metallurgical and Materials Transactions A, 2011, 42(11): 3386-3398.

[48] Dünckelmeyer M, Karelova A, KreMPaszky C, et al. Instrumented hole expansion test[C]//Proceeding of International Doctoral Seminar. 2009: 411-419.

[49] Jieshi Chen, Xianbin Zhou. A new curve fitting method for forming limit experimental data. J. Mater. Sci. Technol. Vol.21 No.4, 2005

[50] Uthaisangsuk V, Prahl U, Münstermann S, et al. Experimental and numerical failure criterion for formability prediction in sheet metal forming[J]. Computational materials science, 2008, 43(1): 43-50.

[51] Yoshida K, Kuwabara T, Kuroda M. Path-dependence of the forming limit stresses in a sheet metal[J]. International Journal of Plasticity, 2007, 23(3): 361-384.

[52] Fang X, Fan Z, Ralph B, et al. Effects of tempering temperature on tensile and hole expansion properties of a C–Mn steel[J]. Journal of materials processing technology, 2003, 132(1): 215-218.

[53] Gom: Material Testing. [WWW] http://www.gom.com/fileadmin/user_upload/industries/flc_fld_EN.pdf

[54] Stoughton T B, Zhu X. Review of theoretical models of the strain-based FLD and their relevance to the stress-based FLD[J]. International Journal of Plasticity, 2004, 20(8): 1463-1486.

[55] Bleck W, Deng Z, Papamantellos K, et al. A comparative study of the forming-limit diagram models for sheet steels[J]. Journal of Materials Processing Technology, 1998, 83(1): 223-230.

[56] Adamczyk R D, Michal G M. Sheared edge extension of high-strength cold-rolled steels[J]. Journal of Applied Metalworking, 1986, 4(2): 157-163.

[57] MAP: MAP Program & Data Library Content. [WWW] http://www.msm.cam.ac.uk/map/map.html

[58] Bhadeshia H K D H. Neural networks in materials science[J]. ISIJ international, 1999, 39(10): 966-979.

[59] Mandal S, Sivaprasad P V, Dube R K. Modeling microstructural evolution during dynamic recrystallization of alloy D9 using artificial neural network[J]. Journal of Materials Engineering and Performance, 2007, 16(6): 672-679.

[60] Fu Z, Mo J, Chen L, et al. Using genetic algorithm-back propagation neural network prediction and finite-element model estimation to optimize the process of multiple-step incremental air-bending forming of sheet metal[J]. Materials & design, 2010, 31(1): 267-277.

[61] Sha W, Edwards K L. The use of artificial neural networks in materials science based research[J]. Materials & design, 2007, 28(6): 1747-1752.

[62] Verlinden B, Duflou J R, Collin P, et al. Cost estimation for sheet metal parts using multiple regression and artificial neural networks: A case study[J]. International Journal of Production Economics, 2008, 111(2): 484-492.

[63] Ghaboussi J, Garrett Jr J H, Wu X. Knowledge-based modeling of material behavior with neural networks[J]. Journal of Engineering Mechanics, 1991, 117(1): 132-153.

[64] Levy B S, Van Tyne C J. Effect of a Strain-Hardening Rate at Uniform Elongation on Sheared Edge Stretching[J]. Journal of materials engineering and performance, 2012, 21(10): 2147-2154.

[65] Kuo T Y, Lin H C. Effects of pulse level of Nd-YAG laser on tensile properties and formability of laser weldments in automotive aluminum alloys[J]. Materials Science and Engineering: A, 2006, 416(1): 281-289.

[66] Narayanasamy R, Narayanan C S, Padmanabhan P, et al. Effect of mechanical and fractographic properties on hole expandability of various automobile steels during hole expansion test[J]. The International Journal of Advanced Manufacturing Technology, 2010, 47(1-4): 365-380.

[67] Chino Y, Mabuchi M, Kishihara R, et al. Mechanical Properties and Press Formability at Room Temperature of AZ31 Mg Alloy Processed by Single Roller Drive Rolling[J]. Materials Transactions, 2002, 43(10): 2554-2560.

[68] Instron: 8801 Fatigue Testing Systems brochure. [WWW] http://www.instron.com/sv-se/products/testing-systems/dynamic-and-fatigue-systems/servohydraulic-fatigue/8801-floor-model

[69] Comstock R J, Scherrer D K, Adamczyk R D. Hole expansion in a variety of sheet steels[J]. Journal of materials engineering and performance, 2006, 15(6): 675-683.

[70] Tampere University of Technology: Scanning Electron Microscopy. [WWW] http://www.tut.fi/en/about-tut/departments/materials-science/research/research-equipment/microscopy/sem/index.htm.

[71] Callister W D, Rethwisch D G. Materials science and engineering: an introduction[M]. New York: Wiley, 2007, pp 134-135.

[72] Raj A K, Padmanabhan K A. Prediction of the formability of metastable low nickel austenitic stainless steel sheets[J]. Journal of Materials Processing Technology, 1999, 94(2): 201-207.

[73] Quiza R, Figueira L, Davim J P. CoMParing statistical models and artificial neural networks on predicting the tool wear in hard machining D2 AISI steel[J]. The International Journal of Advanced Manufacturing Technology, 2008, 37(7-8): 641-648.